Frequency Response Testing in the CIET Facility

Christopher Poresky

UCBTH-17-002

May 2017
Department of Nuclear Engineering
University of California, Berkeley

This research is being performed using funding received from the U.S. Department of Energy Office of Nuclear Energy's Nuclear Energy University Programs.

Abstract

Frequency Response Testing in the CIET Facility
By
Christopher Morris Poresky

This report presents the motivation and methodology for frequency response testing in integral effects tests. Preliminary frequency response testing with sinusoidal inputs across a range of frequencies in the Compact Integral Effects Test was conducted, demonstrating feasibility and potential for insights into conjugate heat transfer between fluid and structural materials. Low-frequency behavior where fluid temperature change lags power input and structural temperature change was observed along with high-frequency behavior where fluid and structural temperature responses become almost perfectly in-phase. The amplitude of temperature response to power input is observed to be frequency-dependent, as is the phase lag. Noticeable limits for dominance of power input to structure heat transfer and fluid-structure heat transfer are observed. Frequency response is calculated using Fast Fourier Transform analysis and its limitations for experimental analysis are explored. Furthermore, a methodology is proposed for using experimental data to determine system parameters including heat transfer coefficients and thermal inertia ratios.

Master's of Science in Nuclear Engineering
University of California, Berkeley

Professor Per F. Peterson, Chair

Acknowledgements

Virtually all experimental work on CIET is conducted with **James Kendrick** as we develop test plans and procedures together, explaining our thoughts and what we hope to gain along the way. Furthermore, he has always taken time out to help me clarify my ideas, run through my analyses, and check my assumptions. This, of course, goes beyond my work on frequency response testing, which has been limited to the past two months. He has made comments and edits to sections of this report, including a description of the CIET control system.

Charalampos Andreades and **Andrew Greenop** have also always graciously offered their time, insight, and perspective on the development of my work. **Dane de Wet**, **Ishak Johnson**, and **Shane Gallagher** have helped me talk through the significance of frequency response testing as well. **Jian Ruan**, although only here for a couple months, always asked tough questions and made sure I knew what I was talking about and could explain it. **Raleigh Lukas** has also conducted exceptional work on CIET, especially on the new heater insert design, fabrication, installation, and testing.

A number of other people assisted me in these last few days of understanding frequency domain analysis, including **Richard Vasquez**, **Kyle Bilton**, and **Franziska Schmidt**.

Finally, I have been very fortunate to receive the support of my professors and advisors. **Scott Moura**, despite not being a professor of the Nuclear Engineering department, has taken his time out on multiple occasions to give me his thoughts about the direction of my research. **Peter Hosemann** has never told me that my questions needed to wait and has always provided humorous and blunt insight on the viability of ideas. Plus, he seems to get really excited about space. **Max Fratoni** probably wishes that his door wasn't so close to where I sit, but has helped me work out a variety of topics, from research to coursework to simply being a grad student. I am grateful to have him as a trusted mentor. Finally, **Per Peterson** has always encouraged my ideas, matching me and raising by at least an order of magnitude, and responded patiently both to frank inquiry and misguided distractions. He has provided me with countless opportunities, taught me that intuition and elegance go hand-in-hand with innovation, and continues to lay forth an inexhaustible supply of possibilities. He has also commented on and edited some sections of this report.

I am constantly delighted by the warmth and approachability of the Berkeley Nuclear Engineering Department. **Thank you.**

Contents

List of Figures

List of Tables

Acronyms and Abbreviations

FHR – Fluoride-salt-cooled high-temperature reactor
MSR – Molten salt cooled and fueled reactor
IET – Integral effects test
CIET – Compact Integral Effects Test
LWR – Light water reactor
MSRE – Molten Salt Reactor Experiment
DRACS – Direct Reactor Auxiliary Cooling System
flibe – Li_2BeF_4
DHX– DRACS heat exchanger
CTAH – Coiled-tube air heat exchanger
TCHX – Thermosyphon-cooled heat exchanger
TC – Thermocouple
DAQ – Data acquisition system
PRBS – Pseudo-Random Binary Sequence
MFBS – Multifrequency Binary Sequence
FFT – Fast Fourier Transform

1 Introduction

1.1 Motivation

The Thermal-Hydraulics Group is continuing the development of test programs for performing design and safety analysis of fluoride-salt-cooled high-temperature reactors (FHRs). Because molten salt cooled and fueled reactors (MSRs) have a coolant that is single-phase under most operating and accident conditions and their coolant and structural materials have large heat capacities, thermal coupling of coolant and structural material is important to dynamic system response. Because FHRs operate at 600-700°C but have fuel thermal limits over 1600°C (much higher than anticipated peak coolant temperatures during transient conditions), thermal-induced material degradation in structural materials is of primary importance for limiting temperature and power. MSRs are unique when compared with other advanced reactor designs because the thermal inertias of their coolant and solid heat structures are similar while remaining single-phase [1].

Integral effects test (IET) experiments can aid in the formulation and validation of theoretical models for a plant to support the safety case, operational considerations, and prototypical design choices. We are using the Compact Integral Effects Test (CIET) Version 2.0 to simulate operation of a representative FHR, conduct verification and validation of best estimate thermal hydraulic system codes, and inform development of a licensing approach for FHRs that uses similar methods already applied in the licensing of passive light water reactor (LWR) designs. Frequency response testing methods may be particularly well-suited to optimizing FHR IET experimental programs due to the single-phase characteristics of FHR coolant and the interaction with solid heat structures.

1.2 History and Background of Frequency Response Testing

Most early frequency response testing in nuclear reactors was conducted on operating research reactors and some power reactors by varying reactivity (moving control rods) using a sinusoidal or pseudo-random binary pulse input. However, for Light Water Reactors, this methodology did not see widespread use. Potential reasons include the strong non-linearity of the phase change and two-phase flow phenomena that occur during LWR accidents, which cannot be studied using frequency response methods that assume primarily linear system response in the operational range.

Test programs that utilized standard plant equipment to generate periodic signals, such as movement of control rods, were conducted in the early 1960s. This focus was used to determine both frequency and impulse response in order to conduct stability analysis. Later developments came with advancements in technology that could simplify and expand the possibilities for signal analysis.

Of particular interest to developers of Molten Salt Reactors and Fluoride-Salt-Cooled High-Temperature Reactors is the work of S. J. Ball and T. W. Kerlin on the Molten Salt Reactor Experiment (MSRE). During its operating life, they analyzed the operational stability of the MSRE and concluded that it was inherently stable. They also drew conclusions about its

transient response at different power levels and were able to make insights into the mechanisms by which the reactor ensures stability. Their analysis was also based on physical models of both heat transfer and neutronics throughout the primary loop [2]. Their test results aided in the creation of a very simple lumped-capacity model that was run on an analog computer. This analog computer model was shown to predict system response quite well, and was used to drive the MSRE control system hardware for testing and training, before the control system hardware was connected to the actual reactor [2]. Later, in 1976, Kerlin et al. conducted frequency response testing at the Oconee pressurized water reactor to identify the reactor's fuel temperature coefficient of reactivity and the overall fuel-to-coolant heat transfer coefficient. These tests were conducted during normal operation with insignificant interference [4].

It has been about 50 years since frequency response testing provided information that could be used both to assess the design of and check current status of operating nuclear reactors. Because molten-salt reactors have similar thermal inertia between fluid and structural materials, the frequency response of fluid and structural temperatures may provide valuable insights into the degradation of structural material due to thermal stress. Furthermore, frequency response testing may be used with more efficiency and more sophisticated analysis now that control technologies, analysis tools, and computational power have increased exponentially.

The frequency response of a signal is determined by examining the relationship between an input and the corresponding output in the variable of interest. For a simple, sinusoidal input signal, we write the input signal, $\delta I(t)$, as:

$$\delta I(t) = b\, sin(\omega t) \tag{1}$$

where t is time, b amplitude, and ω frequency in radians/time. We then measure an output signal, $\delta O(t)$, of the form:

$$\delta O(t) = b|G(j\omega)|\, sin(\omega t + \psi) \tag{2}$$

where $|G(j\omega)|$ is the gain of the output signal, or the proportion between the amplitude of the output and the amplitude of the input at a given frequency. Additionally, ψ is the phase angle of the output sine wave.

The ability to describe this input-output relationship with amplitude and phase angle alone is part of what motivates the use of frequency response testing. The primary motivation for using frequency response testing in experiments involves the ability to extract high-quality data, with low signal-to-noise, to validate system modeling and check mathematical models and parameters used to predict system behavior at both steady-state and transient conditions. Additionally, frequency response testing can be used to tune controllers and to assess system stability during transient conditions [4].

2 CIET Description

The Compact Integral Effects Test (CIET) consists of two coupled flow loops that replicate the integral thermal hydraulic response of FHRs using Direct Reactor Auxiliary Cooling Systems (DRACS), under forced and natural circulation at a scaled height and reduced flow area [6]. By using Dowtherm A heating oil as a simulant fluid for the prototypical FHR coolant, flibe (Li_2BeF_4), this scaling can simulate prototypical FHR performance at significantly reduced temperatures [7]. CIET was originally designed to provide experimental data for verification and validation of best estimate thermal hydraulic models and has been used both for steady-state and transient test cases [6]. Figure 2-1 shows a 3-D model of CIET.

CIET replicates the two major flow paths in a prototypical FHR: the natural circulation DRACS loop and the forced circulation primary loop. The primary loop heat structures are a vertical heated section, the shell side of a vertical single-pass straight shell-and-tube DRACS heat exchanger (DHX), and a variable speed fan-driven air-to-oil heat exchanger used to simulate the coiled-tube air heat exchanger (CTAH). The DRACS loop has the tube side of the DHX and a thermosyphon-cooled heat exchanger (TCHX). Both the TCHX and the CTAH are computer-controlled, variable-speed fan-cooled air-to-oil heat exchangers. TCHX and CTAH outlet temperatures are controlled to desired values using PID controllers. For the experiments discussed in this paper, we focus on the primary loop.

The structural materials in the primary loop of CIET include thin wall (Schedule 10) 304L stainless steel piping, as well as more weakly coupled thermal structures such as flanges and valves. The heater section provides power though copper electrodes that are connected to its outer tube from DC power supplies operating between 0 and 10 kW and controlled through a LabVIEW interface. All of the primary loop, excluding the CTAH, has 5-cm-thick fiberglass insulation to limit heat losses to ambient air. UCB has inspected the insulation for parasitic heat losses under steady-state operation using an infrared camera, and added additional local insulation to reduce localized heat loss. Each loop accommodates volumetric expansion of the fluid using expansion tanks maintained at atmospheric pressure and installed at the uppermost elevation.

Temperatures in CIET are measured with type-T inline thermocouples (TCs) with 0.5-mm-diameter sheaths and ungrounded junctions in direct contact with the Dowtherm coolant, providing very rapid thermal response. Their accuracy is ±0.5°C in the 0-200°C range [6]. Thermocouples are located at the inlets and outlets of each heat structure. In order to ensure that the bulk (mixing cup) temperature can be determined, each measurement position has a TC both at the center and near the wall. A thermowell in the loop contains a NIST-calibrated thermistor, which provides an independent measurement of temperature and which can be used to check thermocouple calibration in-situ by running with isothermal conditions. Coriolis flowmeters with accuracies of ±2% over the range of flow rates tested provide direct measurements of mass flow rates [6].

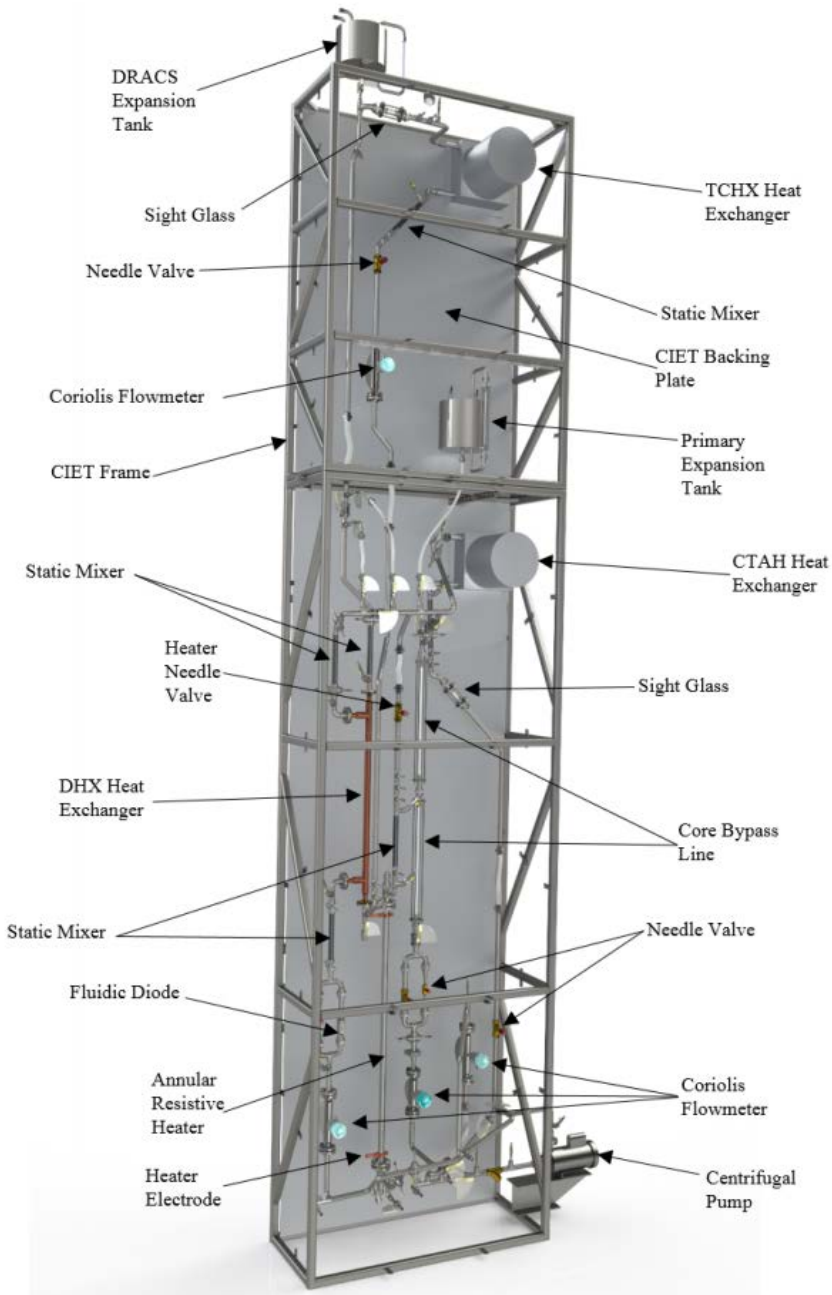

Figure 2-1. 3-D model of CIET showing components and coupled natural circulation loops [7]

Control of heater power input is accomplished using a LabVIEW control system. The temperatures and mass flow rates in each loop are recorded with a National Instruments data acquisition (DAQ) system [6]. Pressure data throughout the loop can be directly measured with manometers and digital cameras, a measurement that would be more difficult at flibe operating temperatures. All data is displayed on a single interface in the LabVIEW front panel. The experimenter also controls CIET using the front panel via buttons and input fields. Here the experimenter has control over the heater, the pump, the CTAH fan, and the TCHX fan by specifying set points or frequencies.

The heater control was designed to produce steady-state output signals with step changes from one steady-state power level to another. This control capability was expanded to include the ability to output sinusoidal signals with the operator controlling the offset, amplitude, and frequency of the sinusoid. However, the performance of the current system is limited to maximum output frequencies of approximately 0.1 Hz. This low oscillation frequency is most likely limited by hardware and control software inside the power supplies that limit maximum power transients. A second limitation is the digital-to-analog conversion from the digital output signal from the control system to the analog power input signal to the system heater which has shown to be fairly coarse, which further limits the output signal frequencies.

3 Experimental Methodology

Frequency response testing requires the experimentalist to choose an input signal that will help reveal and define the corresponding output signal. There are a number of signals to choose from and their selection depends on the test purpose. For example, pseudo-random binary sequency (PRBS) forcing can be used to measure frequency response at multiple harmonic frequencies in one test [4]. There are also variations of the PRBS that can be used to discriminate against nonlinear effects with varying degrees of complexity both in implementation and analysis. The signal that can maximize test efficiency is the Multifrequency Binary Sequence (MFBS), which is the sum of a series of sinusoids at different harmonic frequencies of interest. However, because this signal requires knowledge of specific desired frequencies a priori and requires more complex control programming, we chose discrete sinusoidal signals for preliminary frequency response testing in CIET. While this type of signal previously required expensive, complex equipment and was difficult to implement with analog reactor components, our LabVIEW control system does not have the same issues. We are therefore able to assess the value of frequency response testing with the existing control configuration that allows for definition of amplitude and frequency.

In studying conjugate heat transfer, we have many choices for temperature measurements. However, the transient heat transfer between fluid and solid structures is of particular importance in understanding and predicting the behavior of the electric heater. While most sections of the loop have no heat generation term, the heater section has heat input provided by the resistance heating of the outer heater tube. This tube is instrumented on the surface but is sufficiently thin that we approximate, with high accuracy, negligible temperature difference through the heater wall. Heat is then transferred to the fluid at the inside surface of the tube. The fluid temperature is also measured with thermocouples in the coolant flow stream at the heater outlet. Finally, the heater inner insert has a complex geometry to enhance heat transfer and adds additional nuance to the heater section as compared to a typical section of primary loop piping.

For this preliminary investigation, we treat the heater section as a single control volume with a representative surface temperature and fluid temperature. In reality, there is a significant axial gradient in these temperatures as they are measured from inlet to outlet. However, one of the potential applications of frequency response testing is to aid in identifying simplified system models which facilitate very good first-order approximations of system behavior.

3.1 Heater Capability Test

During preliminary testing to determine the capabilities of the CIET facility for transient experiments, a sinusoidal input power signal was used to study the electric heater's behavior. A number of frequencies and amplitudes were chosen, including 0.0167 Hz, corresponding to an approximation of the residence time of Dowtherm A in the primary loop during nominal operation at a flow rate of 0.18 kg/s. We ran at a variety of amplitudes and frequencies in order to better understand the electric heater's limitations.

Upon examining the data, shown in Figure 3-1, it became apparent that the input power and heater wall temperature are almost perfectly out of phase.

In fact, the heater outlet temperature is also out of phase with the power and the heater wall temperature. Other system temperatures not shown in Figure 3-1 also exhibit phase shifts as well as changes in amplitude as the signal propagates from the heater through the system and energy is absorbed from and desorbed into the system. This indicates not only that the frequency response of loop temperature to input power may be valuable in characterizing system thermal inertia, but also that the relationships between temperatures at different locations in the loop can be studied.

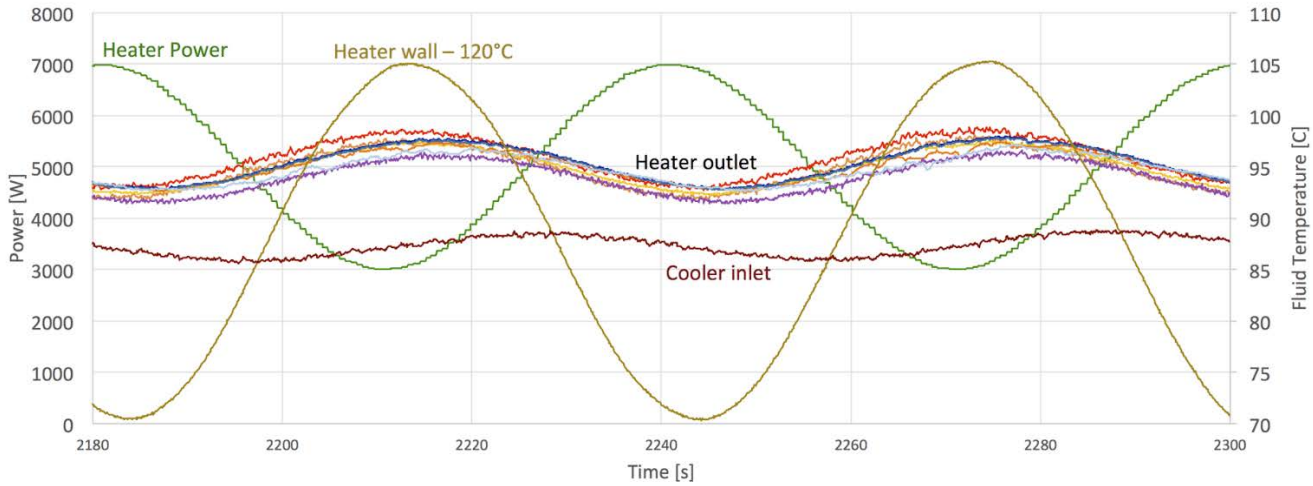

Figure 3-1. Thermal response of heater wall and outlet due to sinusoidal power input.
Note: Heater wall temperature reduced for comparison [Test Data: 2015-08-17 LOFCM Test]

Our observations of these results, coupled with the simultaneous research in frequency response testing conducted by Lakshana Huddar with the Pebble-Bed Heat Transfer Experiment [8], led us to begin exploring frequency response testing in CIET.

3.2 New Heater Insert Testing

The Thermal-Hydraulics Lab has recently replaced the inner tube of CIET's electric heater with a new insert that enhances heat transfer. It is porous, allowing fluid flow through the center of the heater and increasing the heater fluid volume. It also has a twisted tape running through its center to help mixing, trip turbulent flow, and enhance heat transfer. Raleigh Lukas and James Kendrick are primarily responsible for efforts in installing the new insert and characterizing its effect on CIET's heat transfer capabilities.

With the new heater insert, CIET's heat transfer characteristics have changed. This provides further motivation for conducting frequency response testing on CIET's heater to understand the heat transfer effects of the new heater insert. Since the heater insert installation testing was just completed in February 2017, we have conducted only a single frequency response test using CIET.

While it is possible to conduct meaningful frequency response testing across an arbitrary range of frequencies, we choose to center our test plan on values of physical relevance. Thus we

choose to test across five frequencies that cover key thermal time constants for the loop. All of these frequencies are tested in a single experiment using CIET. The desired amplitude and frequency of an input power signal is entered manually in the LabVIEW front panel at each transition time. Table 3-1 lists the step-by-step actions taken in the experiment.

With the current configuration of the electrical heater, CIET can safely be run at 10 kW of power input. In order to make sure that the experiment remains within safe operating limits, a steady-state power of 9 kW is chosen so that sinusoidal signals can be used with an amplitude of 1 kW. The entire experiment is conducted with the nominal mass flow rate of 0.18 kg/s so that the frequency response of the loop temperatures relative to heater oscillation are isolated.

Table 3-1. CIET frequency response test action table

Step	Description	Mass Flow Rate [kg/s]	Heater Power [kW]	CTAH Outlet [°C]	Amplitude [kW]	Frequency [Hz]
1	Increase pump speed to achieve 0.18 kg/s	0.18	0	80	-	-
2	Ramp heater power to 9 kW	0.18	9	80	-	-
3	Set heater to oscillate with an amplitude of 1 kW and an offset of 9 kW: **P(t) = 9 + sin(0.002301t)**	0.18	9	80	1	0.000366
4	**P(t) = 9 + sin(0.02301t)**	0.18	9	80	1	0.00366
5	**P(t) = 9 + sin(0.2301t)**	0.18	9	80	1	0.0366
6	**P(t) = 9 + sin(2.301t)**	0.18	9	80	1	0.366
7	**P(t) = 9 + sin(23.01t)**	0.18	9	80	1	3.66

4 Experimental Results

In this section, CIET experimental results are presented by frequency for both heater output and heater surface temperature along with power versus time. Each temperature is plotted on its own axis to best illustrate its periodic behavior.

A Note on Data Reduction: Select frequencies and amplitudes have been omitted due to their lack of useful information. Examples include tests in which the period was too long and the test was too short to collect sufficient data, or in which the system was not fully at steady state before taking measurements. Additionally, they may not have provided unique information.

4.1 Old Heater Insert

Our heater oscillation experiment with the old heater insert yielded interesting results, as described above. Recently, I have developed a MATLAB .m file which facilitates efficient data analysis. Results for three frequencies are shown below in Figure 4-1, Figure 4-2, and Figure 4-5.

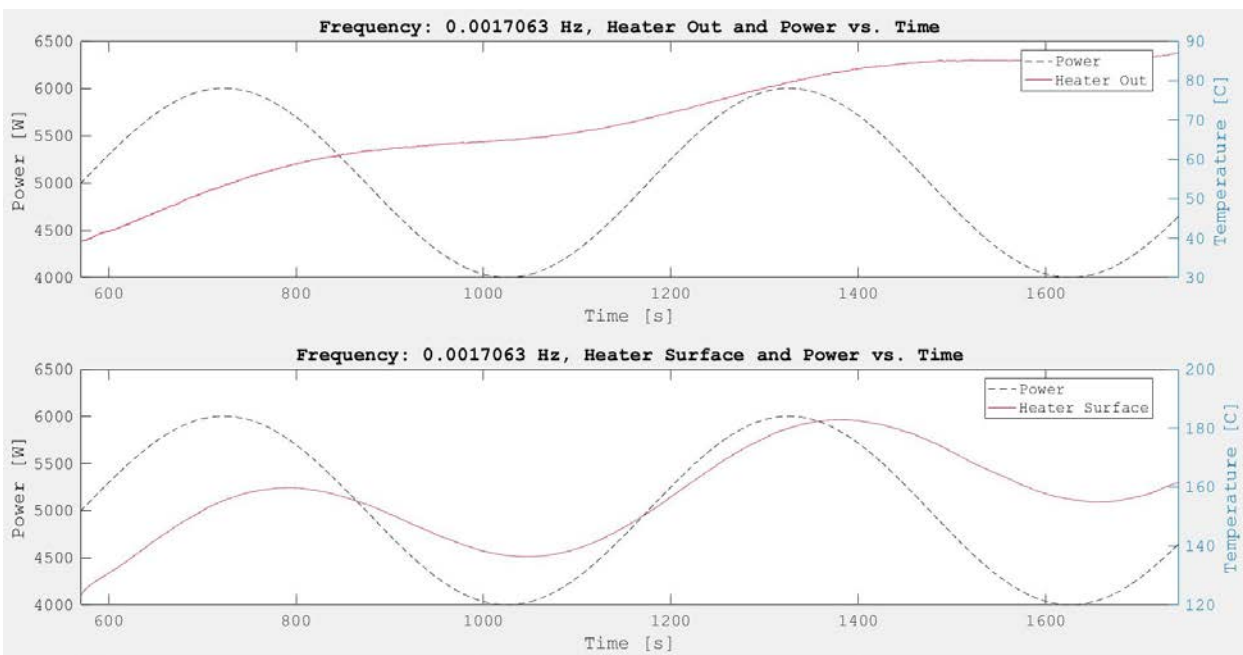

Figure 4-1. Heater outlet, surface temperature, and power vs. time for old heater insert at very low frequency and 1 kW amplitude *[Test Data: 2015-08-17 LOFCM Test]*

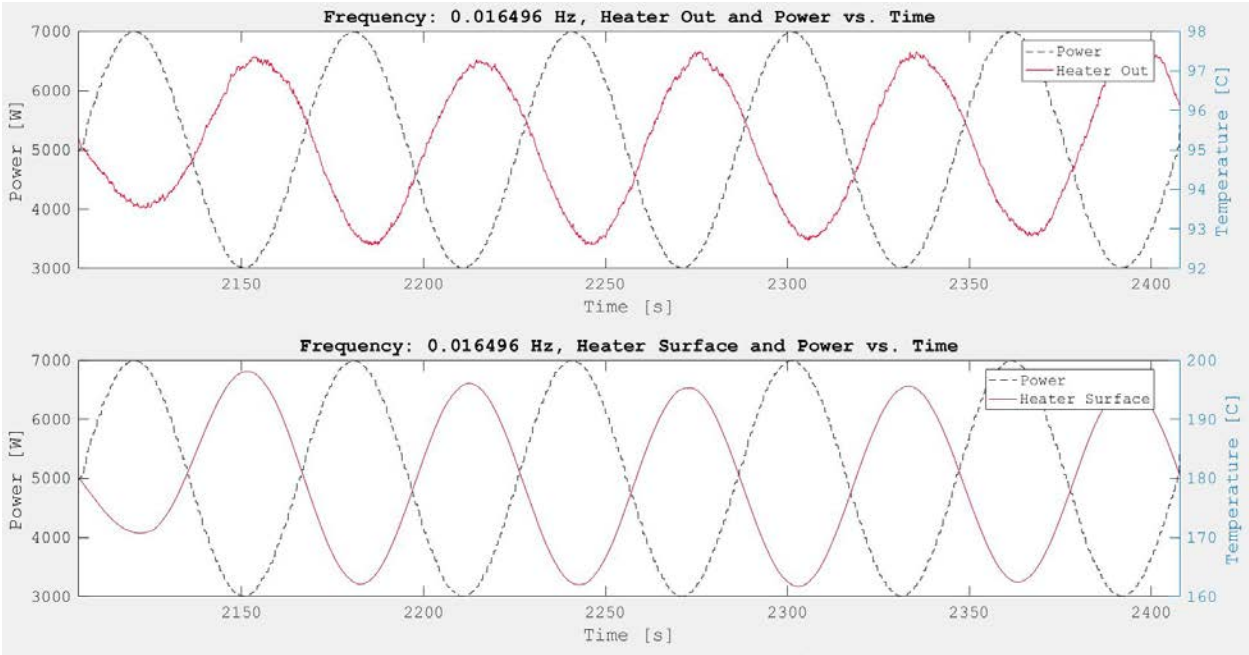

Figure 1-2. Heater outlet, surface temperature, and power vs. time for old heater insert near circulation frequency and 1.5 kW amplitude *[Test Data: 2015-08-17 LOFCM Test]*

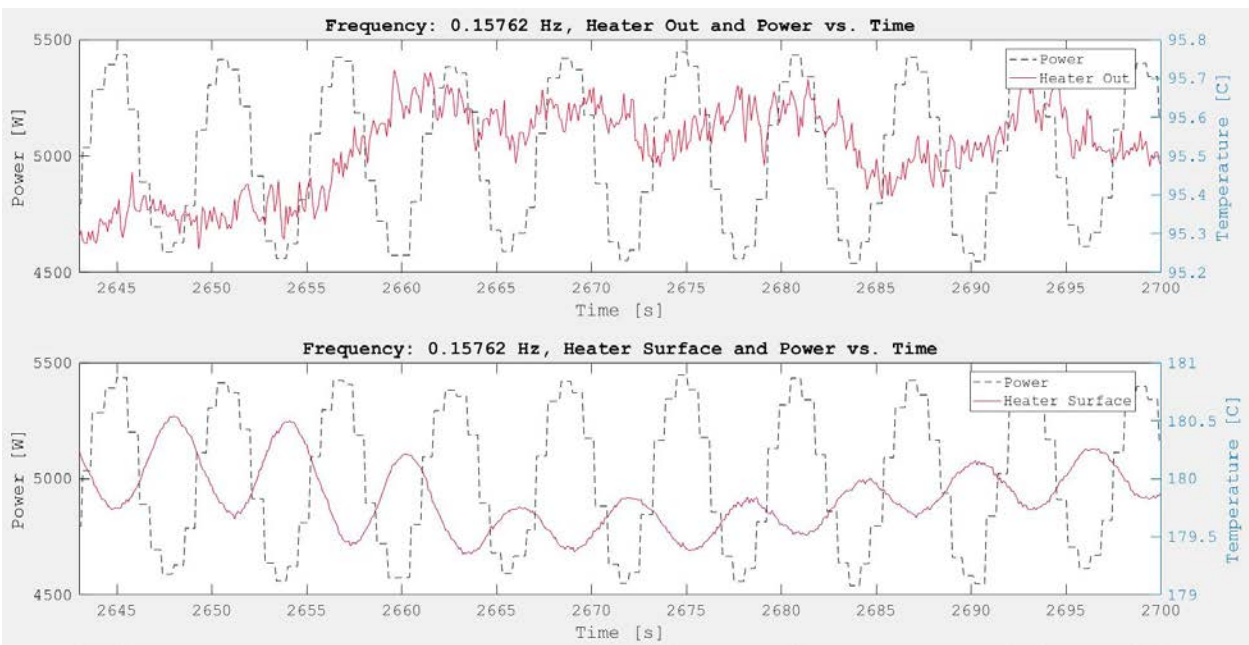

Figure 4-3. Heater outlet, surface temperature, and power vs. time for old heater insert at high frequency and 500 W amplitude *[Test Data: 2015-08-17 LOFCM Test]*

We can clearly see that, at the low frequency shown in Figure 4-1, CIET had not yet reached steady-state, indicating that this data is not very useful. It is, however, included here to illustrate why other frequencies were not included. Figure 4-2 shows a cleaner version of Figure 3-1 in which heater outlet and surface temperatures lag power by what appears to be nearly 180 degrees and have a noticeable amplitude response. Finally, in Figure 4-3, we see that the response of the

heater outlet temperature begins to break down and is unable to keep pace with the heater oscillation, while the heater surface temperature still oscillates, but with very low amplitude.

4.2 New Heater Insert

Upon setting out to conduct this experiment, the lowest frequency was chosen so that it would take about 45 minutes to complete one period of oscillation. However, we quickly realized that the CIET heater was not oscillating with the same frequency we had input. For a frequency of 3.66×10^{-4} Hz entered into the LabVIEW front panel, we saw an actual value of 2.44×10^{-4} Hz, or a signal with roughly 2/3 of the desired frequency. This would have required over an hour to complete one period of oscillation, so this section of the test was curtailed to one-quarter period. The results at this frequency have therefore been omitted because one-quarter period was not enough to identify meaningful frequency response characteristics.

For the second desired frequency of 3.66×10^{-3} Hz, the system actually operated at 4.35×10^{-4} Hz, or about 11.8 % of the desired frequency. This gives a period of about 38 minutes. We operated at this frequency for one period, yielding the data shown in Figure 4-4.

At this second frequency, a phase lag is discernible between the temperatures and the power. In fact, the fluid temperature seems to lag the structural temperature as well, indicating that this frequency may help define an operating regime where heater input to structural material dominates over fluid-structure heat transfer.

The third desired frequency is 3.66×10^{-2} Hz, where the heater actually supplied a signal at 5.75×10^{-3} Hz, or about 15.7 % of the desired frequency once again. This gives a period of about 3 minutes. We operated at this frequency for multiple periods. The results are presented in Figure 4-5.

A phase lag is also clearly shown. At this frequency of oscillation, the amplitude of temperature oscillation actually seems to shrink as compared to the previous frequency, perhaps as the frequency becomes higher than some threshold related to the thermal inertia of the fluid and structural material.

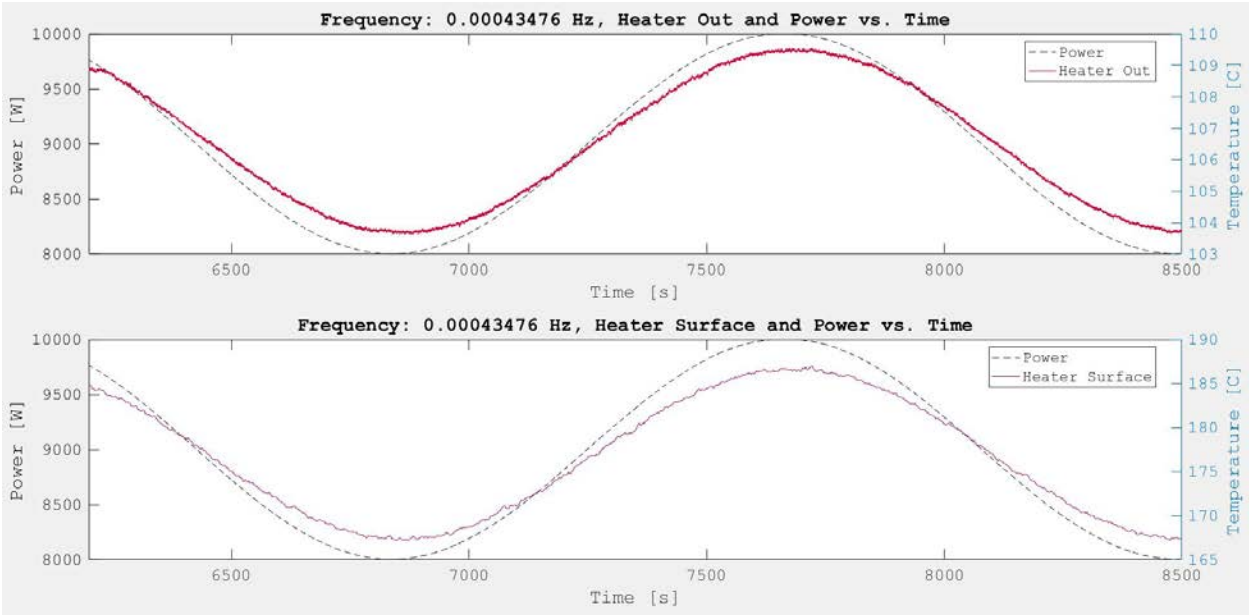

Figure 4-4. Heater outlet, surface temperature, and power vs. time for new heater insert at lowest frequency and 1 kW amplitude
[Test Data: 2017-02-28_Frequency_Response_Heater_Data_raw]

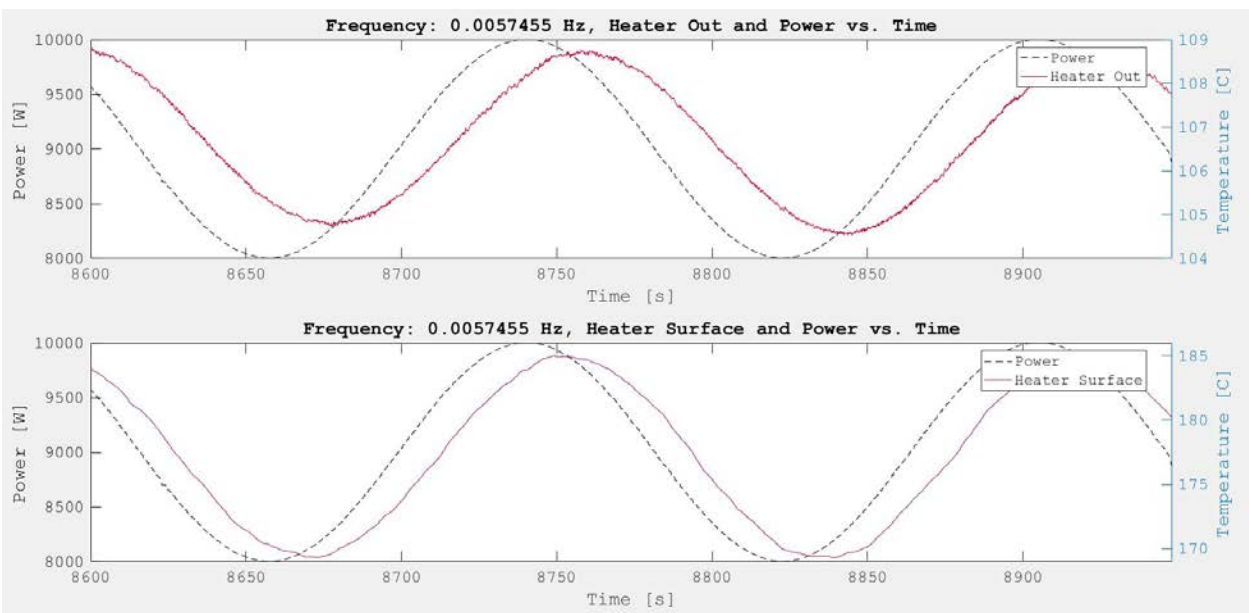

Figure 4-5. Heater outlet, surface temperature, and power vs. time for new heater insert at low frequency and 1 kW amplitude
[Test Data: 2017-02-28_Frequency_Response_Heater_Data_raw]

Ramping up by another order of magnitude, the heater was next set to 0.366 Hz but achieved an actual frequency of 0.0610 Hz, or 16.7% of the desired frequency. Now we have reason to believe that this is a systematic problem that could potentially be anticipated and accounted for in the design of a test plan. The results from this part of the experiment are presented in Figure 4-6.

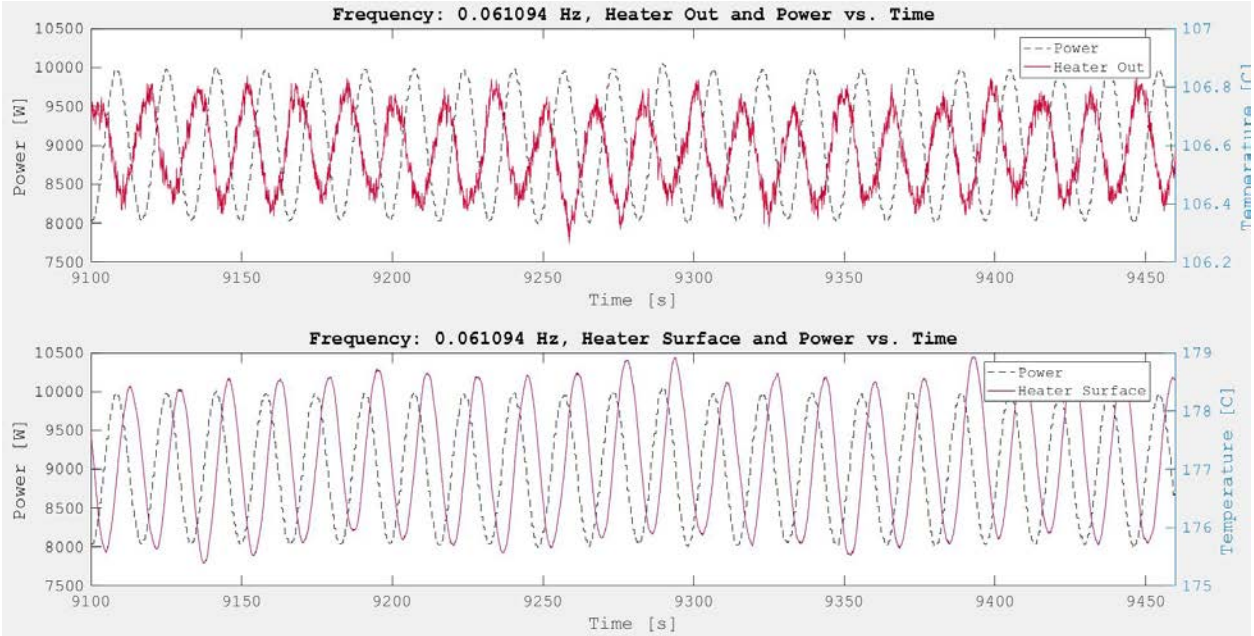

Figure 4-6. Heater outlet, surface temperature, and power vs. time for new heater insert at medium frequency and 1 kW amplitude
[Test Data: 2017-02-28_Frequency_Response_Heater_Data_raw]

At this frequency, we begin to see a significant drop-off in amplitude of both heater output and surface temperature. We also see the most obvious phase lag yet. In fact, it seems as if heater coolant outlet temperature is almost completely out of phase with the power.

The final test frequency was 3.66 Hz but the actual oscillation of the heater turned out to be 0.604 Hz, or about 16.5% of the desired frequency. Figure 4-7 shows the results of the test at this frequency.

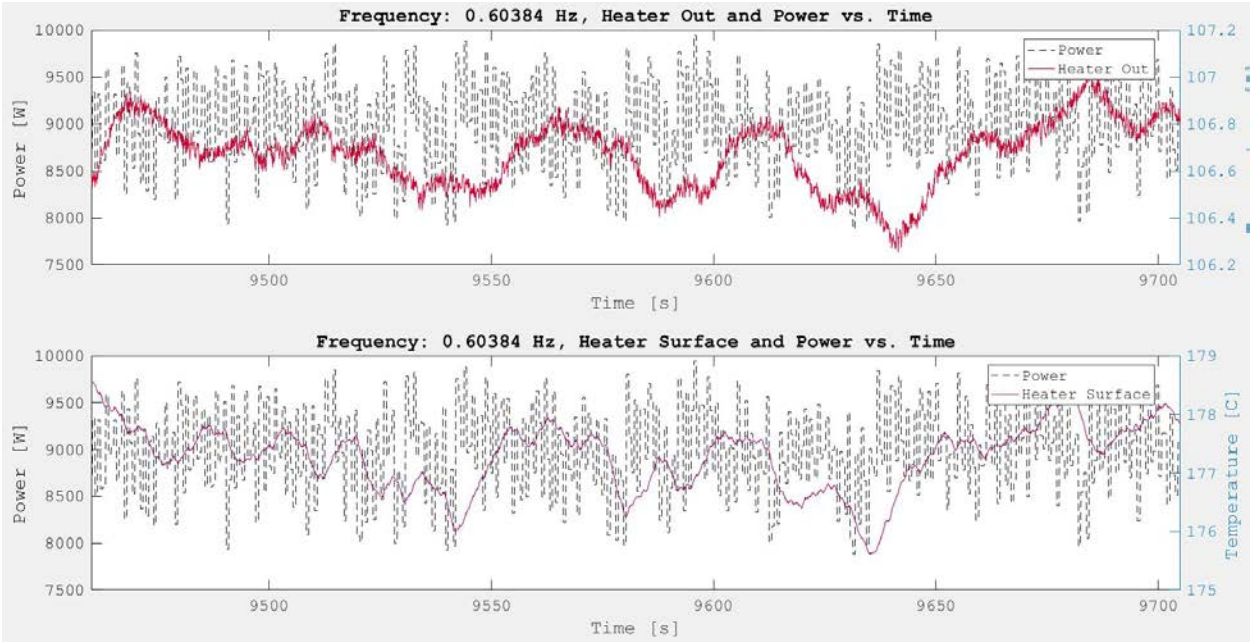

Figure 4-7. Heater outlet, surface temperature, and power vs. time for new heater insert at high frequency and 1 kW amplitude
[Test Data: 2017-02-28_Frequency_Response_Heater_Data_raw]

The most obvious observation that can be made here is that the heater oscillation breaks down near this frequency. We have a limitation on our current control and hardware configuration that the system has difficulty oscillating at frequencies above 0.1 Hz. However, despite the fact that we do not get a "clean" signal, we can still see some semblance of period behavior. We also see that the amplitude of heater outlet temperature becomes comparable to the typical fluctuations we observe during steady-state operation. We see that the heater structural temperature still fluctuates with some noticeable amplitude as expected due to the fact that it is being resistively heated to provide power input.

5 Data Analysis

One benefit of frequency response testing data is that data visualization provides the means for a near-immediate qualitative analysis. However, if the data is to be used for quantitative analysis or, eventually, determination of system parameters, a more precise evaluation of data will need to be performed.

Using a MATLAB script, the experimental data from CIET was extracted from a comma-separated values file, split into loop components and averaged across spatially-distributed thermocouples to give averaged data. After looking at the full test data, the user is then able to specify sub-test start and end times so that the data can be automatically split and categorized by sub-test, plotted, and analyzed.

5.1 Determination of Frequency Domain Characteristics

We then calculate the frequency domain characteristics of the data using Fast Fourier Transforms (FFTs), a computer algorithm for calculating Discrete Fourier Transforms. By using the fft.m function in MATLAB, I was able to input a discrete signal, such as the temperature data from one of the frequencies shown in the previous section, and then specify a sampling frequency (10 Hz for CIET) in order to output a set of amplitude and frequency values. Plotting an FFT of the data gives a set of peaks at frequencies which compose the signal with corresponding amplitudes.

Because we are inputting a simple sinusoidal signal consisting of only one frequency, we expect the same output. However, because we have a constant component (i.e. the steady-state value of power and temperature is not zero, but some positive value), we obtain a massive peak at a frequency of 0 Hz, representing a standing wave. In order to conduct analysis, we need to filter this peak out of our data.

In order to properly inspect the data from these experiments, I first perform an FFT on the data, identify the amplitude of the zero frequency peak, and then perform a new FFT on the data, corrected to subtract this peak value. This allows an automated calculation of the steady-state component and does not require knowledge of the value.

Finally, the peak of this adjusted FFT gives us the dominant frequency. It is important to note that this method of calculation benefits from a few periods of data and that it has poor estimation of frequency domain characteristics for partial oscillations where the periodicity of the signal is not clear.

Once the FFT is obtained, the frequency and corresponding magnitude can be calculated as well as the angle of the frequency domain vector of values. As we further develop our methodology for frequency response testing, I will continue to build the utility of the analysis code to optimize findings from experimental data.

5.2 Frequency Domain Characteristics of the Old Heater Insert

Despite the fact that the only data for the old heater insert is from August 2015, the MATLAB data analysis script allows the user to conduct the same analysis on that data as for the newest data. This is thanks both to our research group's quality assurance and record-keeping efforts, as well as efforts of James Kendrick and myself to standardize our data collection and formatting practices.

Table 5-1 shows the calculated frequency domain characteristics from selected frequencies described in Section 4.1. Included are the frequency of the test, the corresponding period (for clarity), the amplitude, and the phase lag of each signal with respect to the power signal.

Table 5-1. Frequency domain characteristics for old heater insert

Frequency [Hz]	Period	Power Amplitude [W]	Location	Amplitude [°C]	Amp. Ratio	Phase Lag [deg.]	Lag Diff. [deg.)
1.71×10^{-3}	9 min 46 sec	1008	Outlet	14.7	1.04	200.14	3.84
			Surface	14.2		196.30	
1.65×10^{-2}	1 min	985	Outlet	2.50	0.277	204.87	24.56
			Surface	9.01		180.31	
1.58×10^{-1}	6.3 sec	299	Outlet	0.0979	0.389	171.42	165.94
			Surface	0.252		5.48	

As previously discussed, the data for the low frequency is unreliable because the system had not reached a steady-state condition. I have included it here in Table 5-1 to demonstrate how the analysis script requires data of certain conditions in order to extract useful information. This is an important insight for future experimental test plans.

However, the second frequency yields some interesting results. We see a noticeable amplitude difference between the fluid and surface temperatures, indicating a difference in heat transfer. Furthermore, we observe that, while both the heater outlet and the heater surface lag the power oscillation significantly, there is also a large discrepancy between them. This indicates a unique frequency response between the two thermal masses, showing promise for being able to draw conclusions about their impact on transient response.

Finally, at the third frequency, we see that fluid temperature still lags the power oscillation completely with amplitude that is almost negligible. Because the structural temperature is driven by the heater directly, it still oscillates roughly out of phase. However, the calculated phase lag does not seem to match the data by visual inspection. This may be due to the fact that the power oscillation wave is not smooth at this high frequency, leading to inferior results. These and other limitations of FFT analysis will need to be explored to define future test plans.

5.3 Frequency Domain Characteristics of the New Heater Insert

I carried out the same analysis for the new heater insert data at a range of frequencies. Unfortunately, they are not the frequencies at which we planned to collect data due to hardware

limitations, but they will hopefully provide some useful information due to the fact that they cover a range of magnitudes. Table 5-2 summarizes frequency domain data for the new heater insert.

Many of our qualitative observations made above are supported with the data in Table 5-1. Systematically, we see that the amplitude of both temperatures grows at first with increasing frequency before dropping significantly at a certain point. We also see a consistently higher amplitude of temperature oscillation from the heater surface temperature compared to the heater outlet temperature, as expected. The ratio of amplitudes for heater outlet to heater surface temperature is highest at low frequency and decreases as they become out-of-phase. At higher frequencies, when they fall back in-phase, this ratio increases once more as we see significant drop-off in response from the fluid temperature. At low frequencies, the heater outlet temperature lags the power oscillation by significantly more than the heater surface temperature. However, at very high frequency, this difference disappears and the heater outlet and surface temperatures become almost perfectly in phase with one another.

Table 5-2. Frequency domain characteristics for new heater insert

Frequency (Hz)	Period	Location	Amplitude [°C]	Amp. Ratio	Phase Lag [deg.]	Lag Diff. [deg.]
2.44×10^{-4}	1 hr 8 min 2 sec	Outlet	1.41	0.35	5.14	3.33
		Surface	4.03		1.81	
4.35×10^{-4}	38 min 20 sec	Outlet	1.92	0.30	6.49	1.12
		Surface	6.40		5.37	
5.75×10^{-3}	2 min 54 sec	Outlet	1.96	0.26	43.70	15.04
		Surface	7.65		28.66	
6.11×10^{-2}	16.4 sec	Outlet	0.17	0.12	225.37	128.91
		Surface	1.41		96.46	
6.04×10^{-1}	1.66 sec	Outlet	0.10	0.26	52.64	10.61
		Surface	0.38		42.03	

5.4 Comparison between Old and New Heater Inserts

One interesting difference between the old and new heater insert frequency response characteristics is that we see an order of magnitude difference in peak amplitude of heater outlet and surface temperatures. For the old heater insert, this peak occurs at frequencies on the order of 10^{-2} Hz (neglecting the first data set) while it occurs at frequencies on the order of 10^{-3} Hz for the new heater inert. On the other hand, the maximum phase difference between heater outlet temperature and heater structural temperature occurs at frequencies on the order of 10^{-1} Hz for the old heater insert and on the order of 10^{-2} for the new heater insert. These key frequency ranges may indicate dominant heat transfer regimes for the different configurations. Further insight into the physical meaning behind the heater's frequency response is necessary to fully understand the significance of this information.

6 Transfer Functions and Initial Insights

The relationship between an input signal and its corresponding output signal can be represented by a transfer function, usually written as: [4]

$$G(s) = \frac{\delta O(s)}{\delta I(s)} \tag{3}$$

Obtaining this relationship between deviation in output and deviation in input signals is the product of frequency response testing. Transfer functions enable powerful analysis of complex linear feedback systems, helping to restrict changes in one variable due to specific inputs such as modeling error. This makes transfer functions useful for understanding error introduced by simplified models, especially in capturing system dynamics [10]. In order to derive the most benefit from frequency response testing in CIET, theoretical transfer functions need to be developed.

6.1 Modeling the CIET Heater

In modeling the CIET heater, we begin by writing equations for the change in temperature for each section of the heater, divided into inner tube, fluid, and outer shell as shown in Figure 6-1.

$$\frac{d\bar{T}_F}{dt} = \frac{1}{\tau_F}\left(T_{F,in} - \bar{T}_F\right) + \frac{(hA)_T}{\left(Mc_p\right)_F}(\bar{T}_T - \bar{T}_F) + \frac{(hA)_S}{\left(Mc_p\right)_F}(\bar{T}_S - \bar{T}_F) \tag{4}$$

$$\frac{d\bar{T}_T}{dt} = \frac{(hA)_T}{\left(Mc_p\right)_T}(\bar{T}_F - \bar{T}_T) \tag{5}$$

$$\frac{d\bar{T}_S}{dt} = \frac{(hA)_S}{\left(Mc_p\right)_S}(\bar{T}_F - \bar{T}_S) + \frac{P}{\left(Mc_p\right)_S} \tag{6}$$

where subscripts F, T, and S indicate fluid, tube, and shell, respectively, $T_{F,in}$ is inlet fluid temperature, (Mc_p) heat capacity in kW-sec/°C, (hA) mean heat transfer times area in kW/°C, P power generation in the heater shell, t time in seconds, τ transit time, all temperatures are in °C, and overbar indicates mean temperature.

In order to formulate these equations, we take heat transfer to the fluid as averaging over time with inlet fluid temperature, convection between the inner tube and fluid, convection between the shell and fluid, and power generation in the shell.

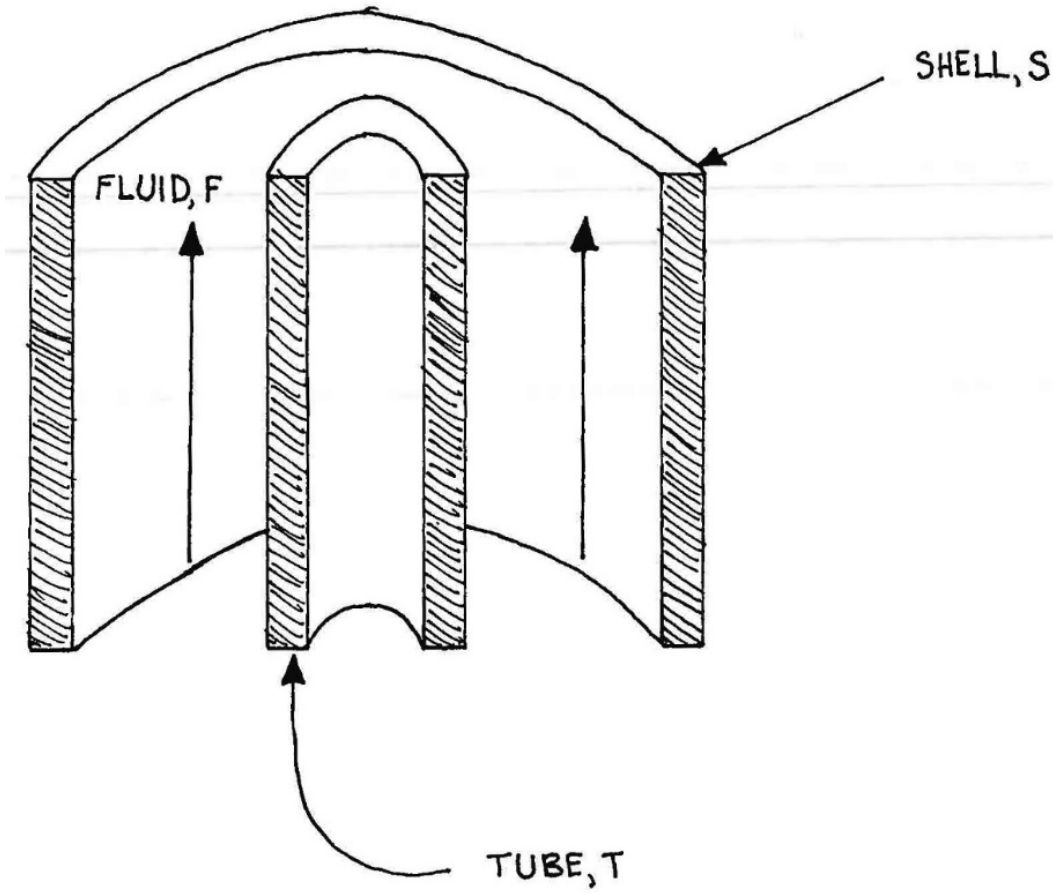

Figure 6-1. Schematic of the CIET heater as a single control volume for modeling purposes

These equations are based on modeling the heater as a single control volume. While the heater shows significant axial variation in temperature, if we are focusing on the inlet and outlet conditions, we may be able to closely approximate its behavior with this simple formulation. One goal of frequency response testing is to determine whether we can use low fidelity models to predict dynamic behavior.

One simplifying assumption we can make is that the fluid and tube are at the same temperature. This is important because we are unable to measure the tube temperature and we also do not know our convection heat transfer coefficients. Fluid, shell, and inlet temperatures are measured. Transit time is a function of flow rate and heater volume. Heat capacities can be calculated from nominal parameters. Power is also measured. While this simplifying assumption may lead to larger discrepancies for the old heater insert, which had no fluid flowing through its center, this may provide a means of defining the difference between the two geometries. Our new, simplified fluid temperature equation becomes:

$$\frac{d\bar{T}_F}{dt} = \frac{1}{\tau_F}\left(T_{F,in} - \bar{T}_F\right) + \frac{(hA)_S}{\left(Mc_p\right)_F}\left(\bar{T}_S - \bar{T}_F\right) \tag{7}$$

6.2 Transfer Function Derivation

Now, to switch to the frequency domain, we use the relationship:

$$\frac{df}{dt} = sF(s) - f(0) \tag{8}$$

where s is the frequency $j\omega$. Assuming all of our variables are deviations from equilibrium values (a valid assumption for sinusoidal functions), we can then arrive at the following frequency domain equations:

$$\hat{\bar{T}}_F = \frac{\frac{1}{\tau_F}\hat{\bar{T}}_{F,in} + \frac{(hA)_S}{(Mc_p)_F}\hat{\bar{T}}_S}{s + \frac{1}{\tau_F} + \frac{(hA)_S}{(Mc_p)_F}} \tag{9}$$

$$\hat{\bar{T}}_S = \frac{\frac{(hA)_S}{(Mc_p)_S}\hat{T}_F + \frac{(hA)_S}{(Mc_p)_F}\hat{P}}{s + \frac{1}{\tau_F} + \frac{(hA)_S}{(Mc_p)_F}} \tag{10}$$

where hat (^) means deviation from equilibrium. Our ultimate goal is to derive equations that isolate our two outputs: fluid and shell temperature, in terms of our two inputs: power and inlet temperature. We can do this for both fluid temperature and shell temperature by substituting (9) and (10) into one another:

$$\hat{\bar{T}}_F = \frac{\frac{1}{\tau_F}\left[s + \frac{(hA)_S}{(Mc_p)_S}\right]\hat{T}_{F,in} + \frac{(hA)_S}{(Mc_p)_F(Mc_p)_S}\hat{P}}{s^2 + \left[\frac{1}{\tau_F} + \frac{(hA)_S}{(Mc_p)_F} + \frac{(hA)_S}{(Mc_p)_S}\right]s + \frac{(hA)_S}{(Mc_p)_S}\left(\frac{1}{\tau_F} - \frac{1}{\tau_F}\frac{(hA)_S}{(Mc_p)_F} + \frac{(hA)_S}{(Mc_p)_F} - \left[\frac{(hA)_S}{(Mc_p)_F}\right]^2\right)} \tag{11}$$

$$\hat{\bar{T}}_S = \frac{\frac{(hA)_S}{(Mc_p)_S}\frac{1}{\tau_F}\hat{T}_{F,in} + \frac{1}{(Mc_p)_S}\left(s + \frac{1}{\tau_F} + \frac{(hA)_S}{(Mc_p)_F}\right)\hat{P}}{s^2 + \left[\frac{(hA)_S}{(Mc_p)_S} + \frac{(hA)_S}{(Mc_p)_F} + \frac{1}{\tau_F} - \frac{(hA)_S}{(Mc_p)_S}\frac{(hA)_S}{(Mc_p)_F}\right]s + \frac{(hA)_S}{(Mc_p)_S}\left[\frac{(hA)_S}{(Mc_p)_F} + \frac{1}{\tau_F} - \frac{(hA)_S}{(Mc_p)_S}\frac{(hA)_S}{(Mc_p)_F}\right]} \tag{12}$$

where we multiply out and collect like terms of s. Because we control our CTAH outlet temperature, we expect that the inlet fluid temperature will have a nearly constant value. Assuming its deviation is zero, we have our outputs in terms of the input power only, and can find our transfer functions. (Note: The details of these derivations can be found in Appendix A.)

$$\boxed{\frac{\hat{\bar{T}}_F}{\hat{P}} = \frac{\frac{(hA)_S}{(Mc_p)_F(Mc_p)_S}}{s^2 + \left[\frac{1}{\tau_F} + \frac{(hA)_S}{(Mc_p)_F} + \frac{(hA)_S}{(Mc_p)_S}\right]s + \frac{(hA)_S}{(Mc_p)_S}\left(\frac{1}{\tau_F} - \frac{1}{\tau_F}\frac{(hA)_S}{(Mc_p)_F} + \frac{(hA)_S}{(Mc_p)_F} - \left[\frac{(hA)_S}{(Mc_p)_F}\right]^2\right)}} \tag{13}$$

$$\boxed{\frac{\hat{\bar{T}}_S}{\hat{P}} = \frac{\frac{1}{(Mc_p)_S}\left(s + \frac{1}{\tau_F} + \frac{(hA)_S}{(Mc_p)_F}\right)}{s^2 + \left[\frac{(hA)_S}{(Mc_p)_S} + \frac{(hA)_S}{(Mc_p)_F} + \frac{1}{\tau_F} - \frac{(hA)_S}{(Mc_p)_S}\frac{(hA)_S}{(Mc_p)_F}\right]s + \frac{(hA)_S}{(Mc_p)_S}\left[\frac{(hA)_S}{(Mc_p)_F} + \frac{1}{\tau_F} - \frac{(hA)_S}{(Mc_p)_S}\frac{(hA)_S}{(Mc_p)_F}\right]}} \tag{14}$$

6.3 Bode Analysis

Now that we have transfer functions for power to fluid temperature and power to shell temperature, we can see what they tell us about our system. The zeros (roots of the numerator) and poles (roots of the denominator) gives us important information about frequencies of interest.

6.3.1 Fluid Temperature

Starting with (13), we see that we have no zeros but that we have poles. We factor the quadratic in the denominator to find our poles:

$$\frac{\hat{\bar{T}}_F}{\hat{P}} = \frac{(hA)_S}{(Mc_p)_F (Mc_p)_S} \frac{1}{\left(s + \frac{1}{\tau_F} + \frac{(hA)_S}{(Mc_p)_F}\right)\left(s + \left[\frac{(hA)_S}{(Mc_p)_F} - 1\right]\frac{(hA)_S}{(Mc_p)_S}\right)} \tag{15}$$

Which means that we have poles at

$$p_1 = -\frac{1}{\tau_F} - \frac{(hA)_S}{(Mc_p)_F} \tag{16}$$

and

$$p_2 = -\left[\frac{(hA)_S}{(Mc_p)_F} - 1\right]\frac{(hA)_S}{(Mc_p)_S} \tag{17}$$

and the static gain, K, can be calculated by setting $s = 0$ so

$$K = \frac{1}{(Mc_p)_F \left(\frac{1}{\tau_F} + \frac{(hA)_S}{(Mc_p)_F}\right)\left(\frac{(hA)_S}{(Mc_p)_F} - 1\right)} \tag{18}$$

and because we know that all of our parameters are real, nonzero, positive values, we know that we have a real, positive pole at p_1 and a real, negative pole at p_2 (because convective heat transfer to the heater outer shell is almost certainly less than the thermal mass of the fluid). On a Bode magnitude plot of this frequency response, each real pole decreases the slope of the magnitude by 20 dB. On a Bode phase plot, negative zeros and positive poles will increase the angle while positive zeros and negative poles will decrease the angle. We will also see the static gain K (which should also be negative when converted to dB) on the Bode magnitude plot of the frequency response at frequencies below p_1 and p_2.

By looking up material, thermal, and geometry properties, we can find example values for our static gain and poles. Until we have the numerical value for our heat transfer coefficient, we cannot actually generate Bode plots from this transfer function. We can, however, use an approximation of the values to draw a generic magnitude plot, shown in Figure 6-2.

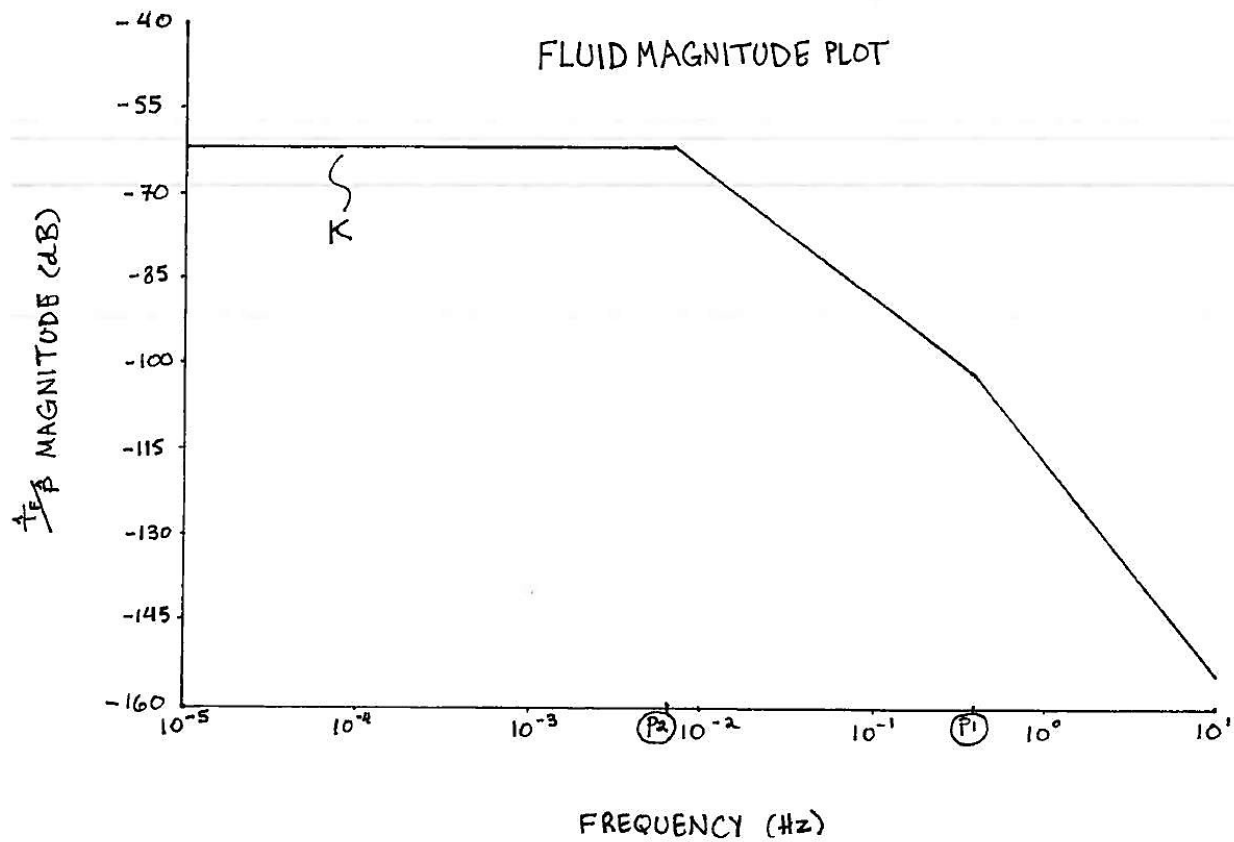

Figure 6-2. General structure of Bode magnitude plot for the transfer function for input power and output mean fluid temperature

Figure 6-2 shows the likely relative magnitudes of p_1 and p_2. We can compare experimentally-determined Bode plots to this general plot and match inflection points and the static gain in order to determine their values and solve equations much simpler than the transfer function. This proves a powerful technique for determining multiple parameters with a single dataset and even for checking uncertain values. For example, we see that the static gain should be represented clearly by a straight line of zero slope before reaching p_2.

Figure 6-3 shows the corresponding generic phase plot, which also facilitates the determination of parameters from our transfer function. This is a method that was employed for reactivity feedback coefficient measurements at the Oconee Power Plant in the 1970s [4]. We can then follow a similar process for the shell temperature.

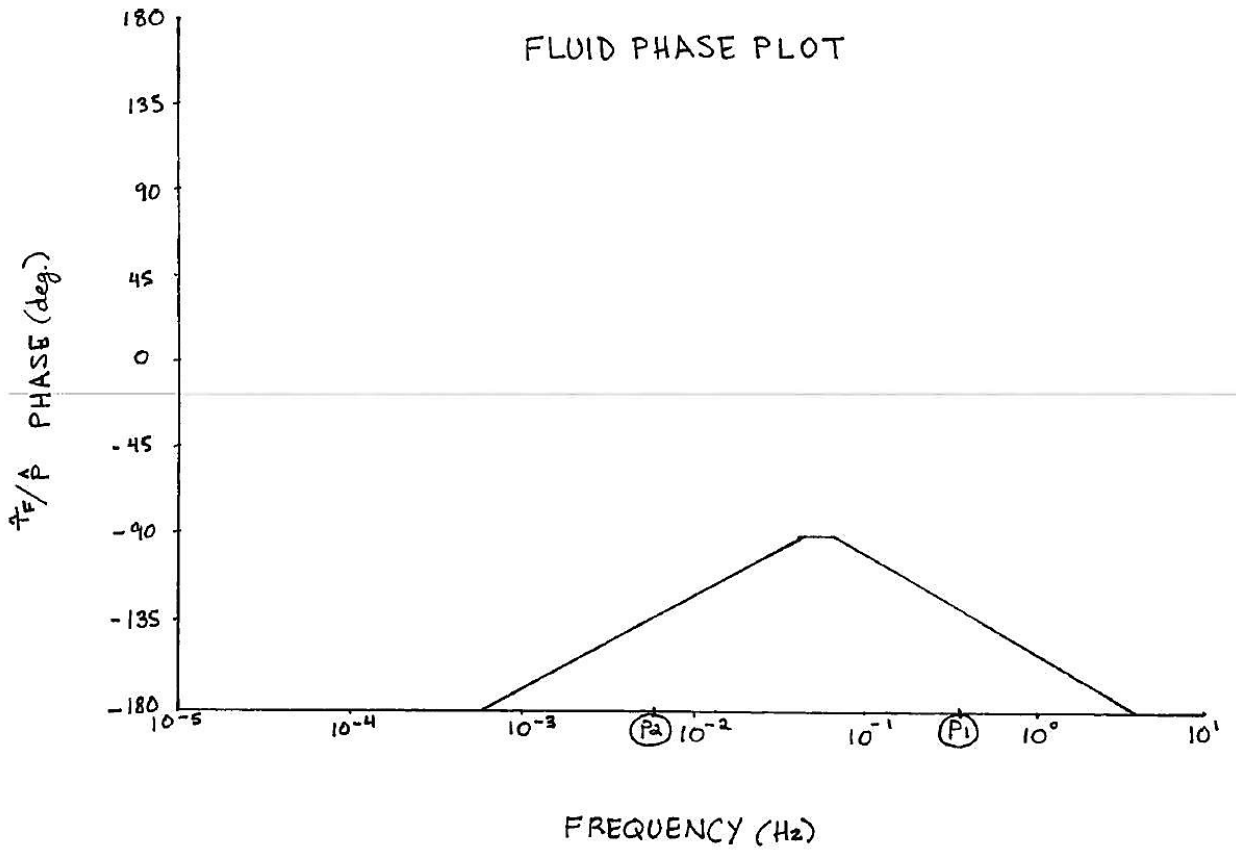

Figure 6-3. General structure of Bode phase plot for the transfer function for input power and output mean fluid temperature

6.3.2 Shell Temperature

Starting with (14), we see that we have a zero and two poles:

$$\frac{\hat{\bar{T}}_S}{\hat{P}} = \frac{1}{(Mc_p)_S} \frac{s + \frac{1}{\tau_F} + \frac{(hA)_S}{(Mc_p)_F}}{\left(s + \frac{(hA)_S}{(Mc_p)_S}\right)\left(s - \left[\frac{(hA)_S}{(Mc_p)_S} - 1\right]\frac{(hA)_S}{(Mc_p)_F} + \frac{1}{\tau_F}\right)} \tag{19}$$

$$z_1 = -\frac{1}{\tau_F} - \frac{(hA)_S}{(Mc_p)_F} \tag{20}$$

$$p_1 = -\frac{(hA)_S}{(Mc_p)_S} \tag{21}$$

$$p_2 = \left[\frac{(hA)_S}{(Mc_p)_S} - 1\right]\frac{(hA)_S}{(Mc_p)_F} - \frac{1}{\tau_F} \tag{22}$$

and static gain

$$K = \frac{\frac{1}{\tau_F} + \frac{(hA)_S}{(Mc_p)_F}}{(hA)_S\left(\frac{1}{\tau_F} - \left[\frac{(hA)_S}{(Mc_p)_S} - 1\right]\frac{(hA)_S}{(Mc_p)_F}\right)} \tag{23}$$

We then draw the generic Bode plot shown in Figure 6-4 and Figure 6-5. Just as with the mean fluid temperature, we can use experimental results to compare with this generic plot and identify our values of interest. One check we can perform is that K for the structural temperature consists of only nominal values.

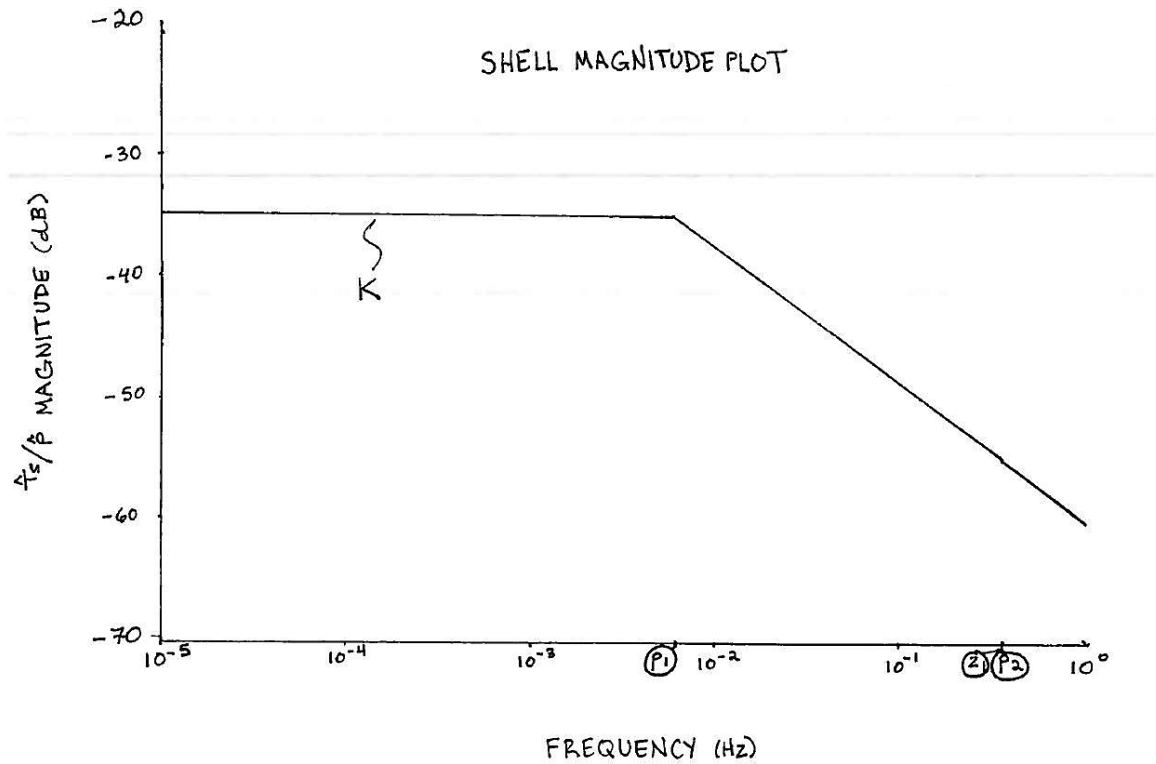

Figure 6-4. General structure of Bode magnitude plot for the transfer function for input power and output mean shell temperature

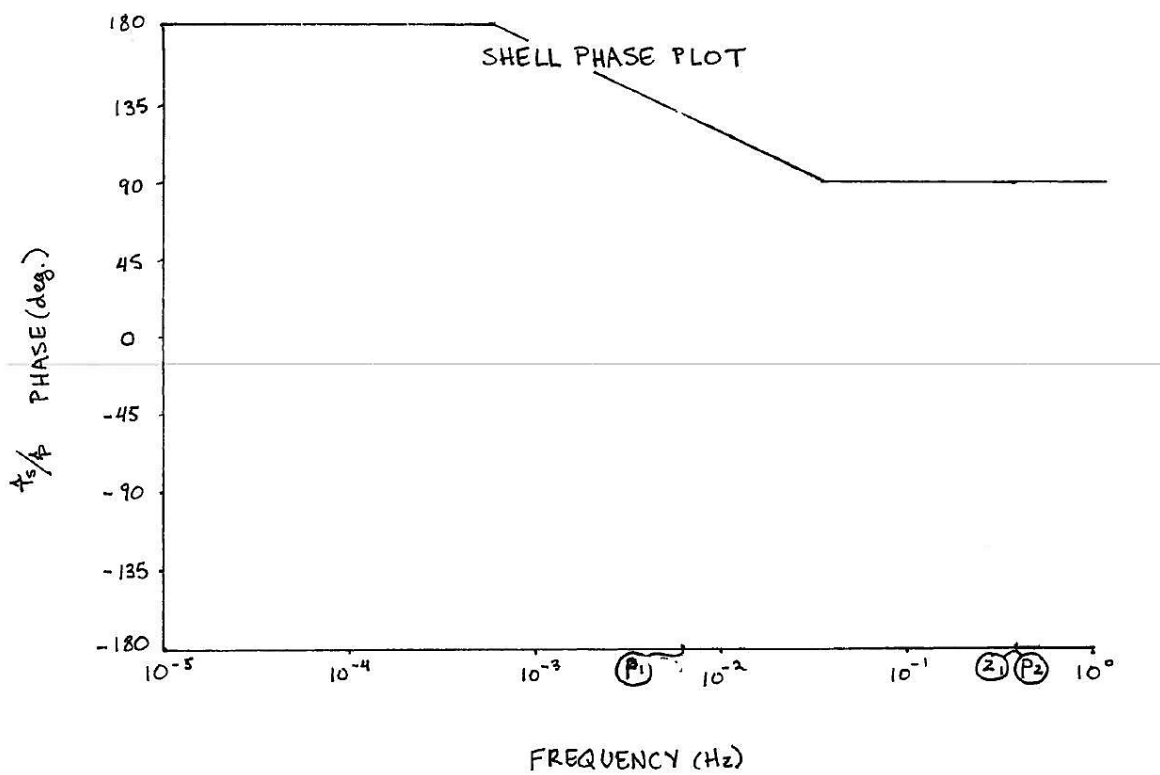

Figure 6-5. General structure of Bode phase plot for the transfer function for input power and output mean shell temperature

6.3.3 Example Values

We can generate more specific example Bode plots by defining the value of the convection coefficient. By this method, we can see the effect of different parameter values (such as tube mass) and even compare with experimental data to check that our assumptions are indeed valid to a first order approximation. We then build our transfer functions in MATLAB and use the built-in bode.m tool to generate Bode magnitude and phase plots. Plots for the old heater are shown in Figure 6-6.

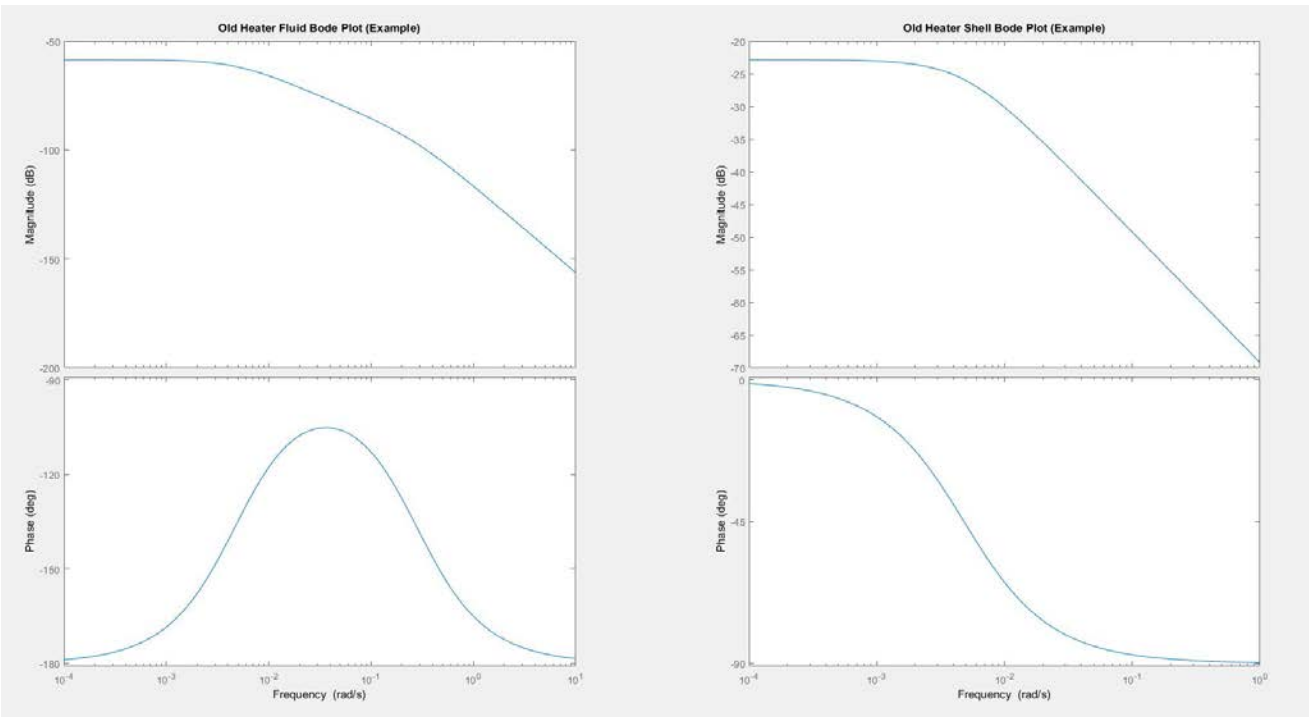

Figure 6-6. Example Bode Magnitude and Phase plots for the old heater insert

For comparison, Figure 6-7 shows the experimental data on the same scale. There is some general agreement, where the MATLAB plots look something like lines of best fit, but more rigorous, numerical analysis is needed. One difference in particular is that the experimental phase plot for the shell temperature shows a phase peak, indicating the presence of a negative zero or positive pole, which is not intuitive when looking at the generic hand-drawn plots. One other observation is that the phase is off, or at least not calibrated correctly. We will need to further investigate our methods for determining phase. However, the main takeaway from this comparison is that our method has potential and we will continue to pursue its use.

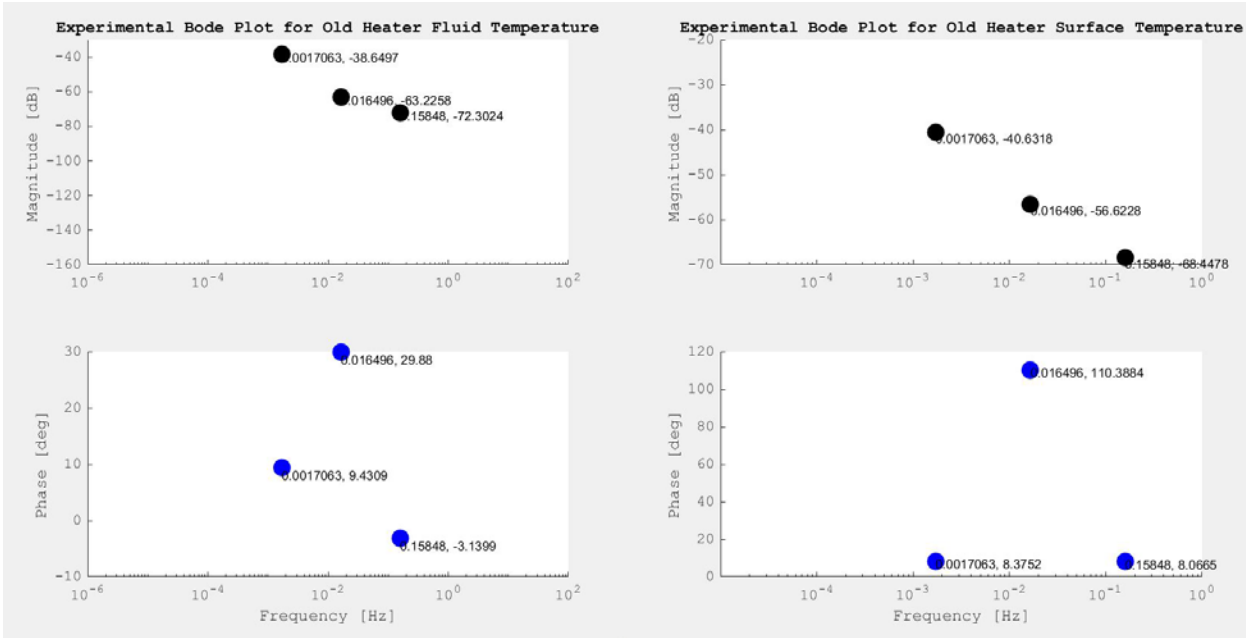

Figure 6-7. Experimental Bode plots for old heater

Example MATLAB Bode plots for the new heater insert are shown in Figure 6-8.

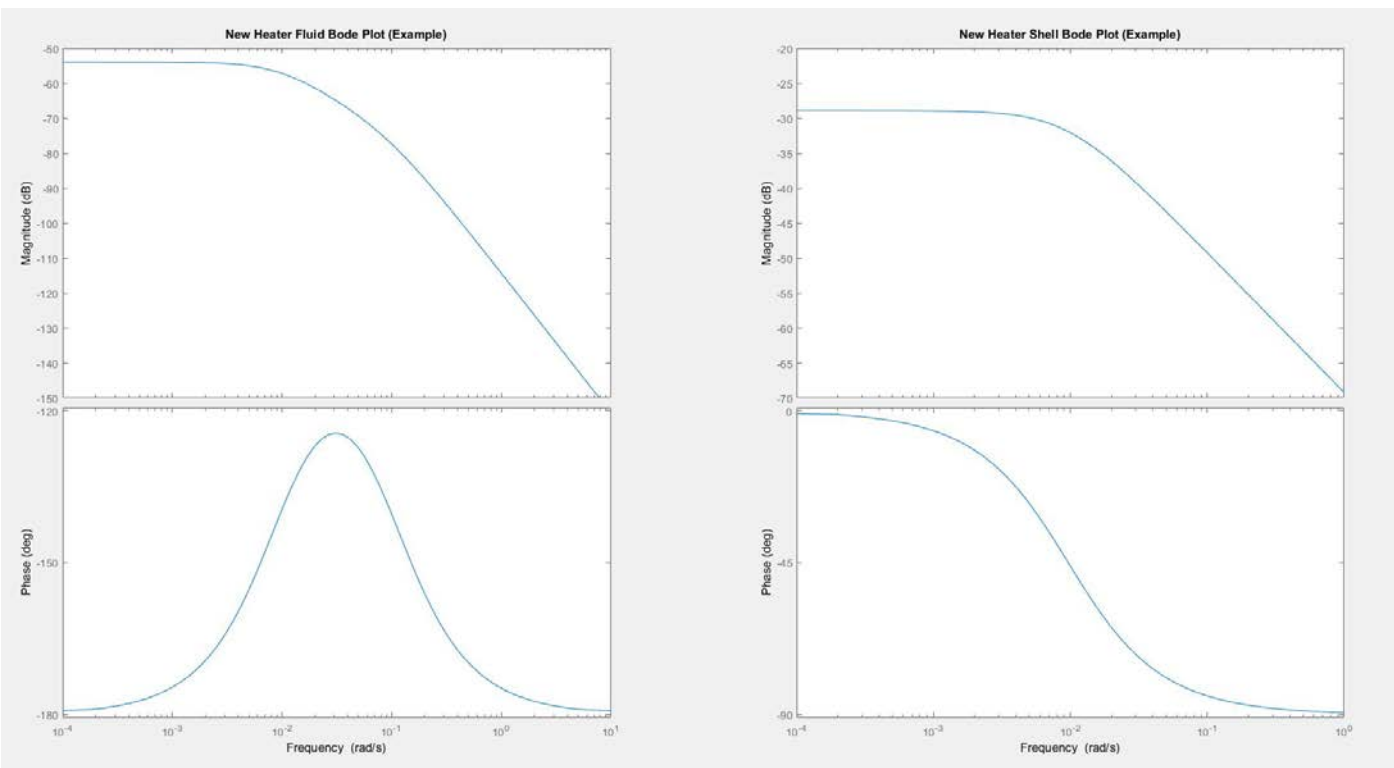

Figure 6-8. Example Bode Magnitude and Phase plots for the new heater insert

These look very similar to the Bode plots for the old heater configuration, meaning that our parameter ratios retain some proportionality across configurations. The main difference in shape is that one of the poles and the zero are actually of the same magnitude, effectively equalizing their effect on the shape. The experimental results are shown in Figure 6-9.

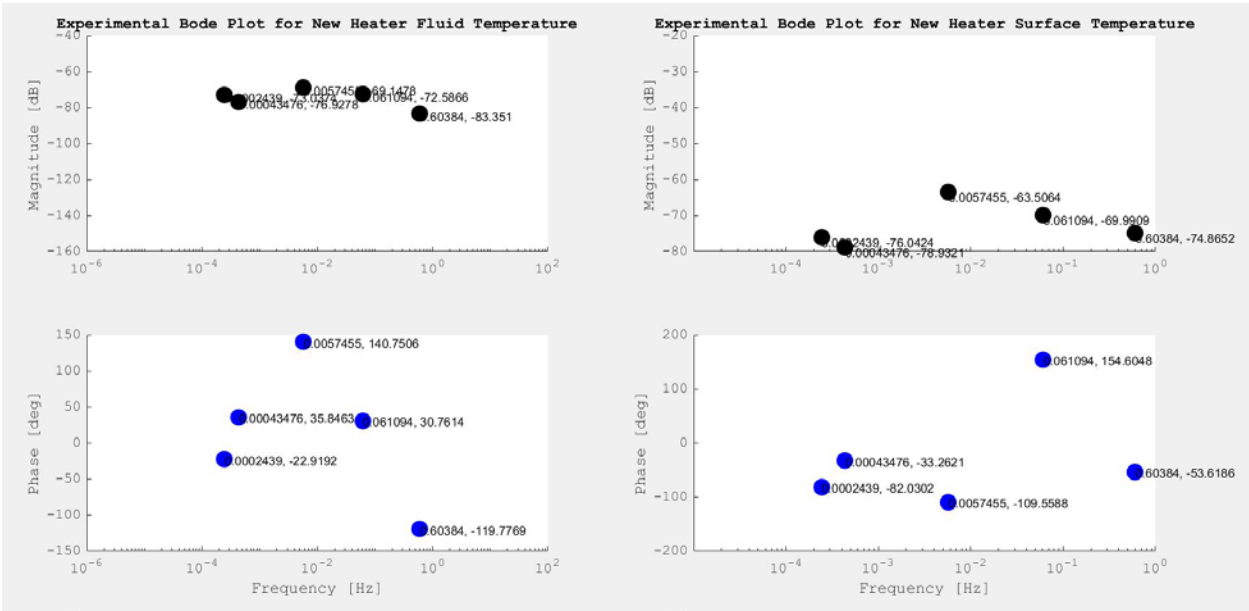

Figure 6-9. Experimental Bode plots for new heater

The agreement here is not as clear as for the old heater, but the general shape is the same. Luckily, with the new heater configuration we have the opportunity to collect as much data as we want. These preliminary results provide motivation for more detailed experiments centered on the frequency ranges we've identified.

7 Conclusions and Future Work

Preliminary frequency response testing with sinusoidal heater power oscillation has shown the potential and demonstrated the methodology for extracting information about conjugate heat transfer between fluid and structural materials in the CIET facility. Data has been presented across multiple magnitudes of frequencies, demonstrating operating regimes where power input to structural material dominates and where heat transfer between structural material and fluid dominates. These relationships have been illustrated through visual inspection as well as calculation of amplitude and phase lag data, facilitating the isolation of important transient thermal inertia behavior. Frequency response testing has also revealed hardware and software limitations that may give insights into considerations for other test plans.

Furthermore, simple physical models have been developed that will facilitate the identification of system parameters such as heat transfer coefficients. We can then compare the viability and efficiency of frequency response analysis with traditional test programs consisting of step change input and an exhaustive set of operating conditions.

7.1 Further Tests

These results provide guidance for planning future frequency response testing as well as deeper analysis to extract more useful information out of each test. We will be able to conduct more targeted testing for frequencies of interest. We will also investigate the benefits of other types of signals, such as MFBS for testing a variety of frequencies more efficiently and the PRBS for recreating test conditions in which oscillations are induced by analog reactor systems like control rods.

Additionally, there are other input-output relationships we can investigate. In the near-term, we can examine the effect of simulated reactivity feedback on system power and temperatures, with an emphasis on stability analysis. This path forward is enabled by the work of visiting scholar Jian Ruan from the Shanghai Institute of Applied Physics and James Kendrick through their implementation of point reactor kinetics models in the CIET control system via MATLAB. Pump frequency or flow rate oscillation may also be an interesting input.

7.2 Model Validation

Once system parameters such as heat transfer coefficients, thermal inertia relationships, and time constants are determined, the ability of simple models to predict dynamic system response can be validated. Of particular interest is the best-estimate thermal-hydraulic system code RELAP5-3D, which may not be able to reproduce smooth sinusoidal forcing. Frequency response model validation may prove very efficient in identifying model shortcomings and ensuring future reliability.

7.3 State Estimation and Fault Detection

Once the system parameters have been identified, we can implement algorithms to predict system state evolution. We may even be able to use this state estimation technique on-line,

allowing for system health monitoring and dynamic decision-making. This opens up the possibility for complementing CIET's measurement capabilities using physics-based models.

Finally, this new set of tools for understanding CIET may lead into fault detection studies in which intelligent, dynamic thresholds can be used to forestall system degradation before it becomes a significant operational concern. This may prove valuable in upcoming research efforts for cyber security in advanced nuclear reactors. Ultimately, CIET is a thermal-hydraulic test loop and these lessons and their implications resonate in a variety of other fields, where efficiency improvements lead to substantial operational rewards.

8 Support

This material is based upon work supported under an Integrated University Program Graduate Fellowship. Any opinions, findings, conclusions or recommendations expressed in this publication are those of the author(s) and do not necessarily reflect the views of the Department of Energy Office of Nuclear Energy.

9 References

1. L. Huddar and et.al., "Application of Frequency Response Methods in Separate and Integral Effects Tests for Molten Salt Cooled and Fueled Reactors," in *HTR 2016*, Las Vegas, NV, 2016.

2. T. Kerlin and S. Ball, "Stability Analysis of the Molten-Salt Reactor Experiment," Oak Ridge National Laboratory, Oak Ridge, TN, 1965.

3. S. Ball, "Simulators for Training Molten-Salt Reactor Experiment Operators," Oak Ridge National Lab, Oak Ridge, TN, 1966.

4. T. Kerlin and et.al., "Dynamic Testing in Nuclear Power Plants for Model Validation," *Journal of Dynamic Systems, Measurement, and Control,* pp. 340-347, 1976.

5. T. Kerlin, Frequency Response Testing in Nuclear Reactors, New York and London: Academic Press, 1974.

6. N. Zweibaum and et.al., "Design of the compact integral effects test facility and validation of best-estimate models for fluoride salt-cooled high-temperature reactors," *Nuclear Technology,* vol. 196, no. 3, pp. 641-660, 2016.

7. P. Peterson and P. Bardet, "Options for Scaled Experiments for High Temperature Liquid Salt and Helium Fluid Mechanics and Convective Heat Transfer," *Nuclear Technology,* vol. 163, pp. 344-357, 2008.

8. N. Zweibaum, "Experimental Validation of Passive Safety System Models: Application to Design and Optimzation of Fluoride-Salt-Cooled, High-Temperature Reactors," PhD Dissertation, University of California, Berkeley, Berkeley, CA, 2015.

9. L. Huddar, "Heat Transfer in Pebble-Bed Nuclear Reactor Cores Cooled by Fluoride Salts, PhD Dissertation," University of California, Berkeley, Berkeley, CA, 2016.

10. Astrom and Murray, Feedback Systems, Princeton and Oxford: Princeton University Press, 2009.

APPENDIX A

CIET Frequency Response Testing: Theory Development

Christopher Poresky

November 15, 2017

Modeling the Heater

We begin by writing equations for the change in temperature for each section of the heater, divided into inner tube, fluid, and outer shell.

$$\frac{d\bar{T}_F}{dt} = \frac{1}{\tau_F}(T_{F,in} - \bar{T}_F) + \frac{(hA)_T}{(Mc_p)_F}(\bar{T}_T - \bar{T}_F) + \frac{(hA)_S}{(Mc_p)_F}(\bar{T}_S - \bar{T}_F) \tag{1}$$

$$\frac{d\bar{T}_T}{dt} = \frac{(hA)_T}{(Mc_p)_T}(\bar{T}_F - \bar{T}_T) \tag{2}$$

$$\frac{d\bar{T}_S}{dt} = \frac{(hA)_S}{(Mc_p)_S}(\bar{T}_F - \bar{T}_S) + \frac{P}{(Mc_p)_S} \tag{3}$$

where

- $\bar{T}_F$ = mean fluid temperature in "well-stirred tank" $[°C]$
- τ_F = transit time for fluid $[sec]$
- t = time $[sec]$
- $T_{F,in}$ = inlet fluid temperature $[°C]$
- $(Mc_p)_F$ = heat capacity of fluid $[kW \cdot sec/°C]$
- $(hA)_T$ = mean heat transfer coefficient times area for fluid-to-tube heat transfer $[kW/°C]$
- $\bar{T}_T$ = mean tube temperature $[°C]$
- $(hA)_S$ = mean heat transfer times area for fluid-to-shell heat transfer $[kW/°C]$
- $\bar{T}_S$ = mean shell temperature $[°C]$
- $(Mc_p)_T$ = heat capacity of tube $[kW \cdot sec/°C]$
- P = power generation in heater outer shell $[kW]$
- $(Mc_p)_S$ = heat capacity of shell $[kW \cdot sec/°C]$

Now comes the fun part. In order to switch to the frequency domain, we use the relationship:

$$\frac{df}{dt} = sF(s) - f(0) \tag{4}$$

Assuming all of our variables are deviations from equilibrium values, we can then write:

$$s\hat{\bar{T}}_F = \frac{1}{\tau_F}(\hat{T}_{F,in} - \hat{\bar{T}}_F) + \frac{(hA)_T}{(Mc_p)_F}(\hat{\bar{T}}_T - \hat{\bar{T}}_F) + \frac{(hA)_S}{(Mc_p)_F}(\hat{\bar{T}}_S - \hat{\bar{T}}_F) \tag{5}$$

$$s\hat{\bar{T}}_T = \frac{(hA)_T}{(Mc_p)_T}(\hat{\bar{T}}_F - \hat{\bar{T}}_T) \tag{6}$$

$$s\hat{\bar{T}}_S = \frac{(hA)_S}{(Mc_p)_S}(\hat{\bar{T}}_F - \hat{\bar{T}}_S) + \frac{\hat{P}}{(Mc_p)_S} \tag{7}$$

Solving the equations for their respective variables:

$$\hat{\bar{T}}_F = \frac{\frac{1}{\tau_F}\hat{T}_{F,in} + \frac{(hA)_T}{(Mc_p)_F}\hat{\bar{T}}_T + \frac{(hA)_S}{(Mc_p)_F}\hat{\bar{T}}_S}{s + \frac{1}{\tau_F} + \frac{(hA)_T}{(Mc_p)_F} + \frac{(hA)_S}{(Mc_p)_F}} \tag{8}$$

$$\hat{\bar{T}}_T = \frac{\frac{(hA)_T}{(Mc_p)_T}\hat{\bar{T}}_F}{s + \frac{(hA)_T}{(Mc_p)_T}} \tag{9}$$

$$\hat{\bar{T}}_S = \frac{\frac{(hA)_S}{(Mc_p)_S}\hat{\bar{T}}_F + \frac{1}{(Mc_p)_S}\hat{P}}{s + \frac{(hA)_S}{(Mc_p)_S}} \tag{10}$$

We can now substitute (9) and (10) into (5) to put $\hat{\bar{T}}_F$ into terms of the inputs $\hat{T}_{F,in}$, $\hat{P}_T$, and the measured $\hat{\bar{T}}_S$ only:

$$s\hat{\bar{T}}_F = \frac{1}{\tau_F}(\hat{T}_{F,in} - \hat{\bar{T}}_F) + \frac{(hA)_T}{(Mc_p)_F}\left(\frac{\frac{(hA)_T}{(Mc_p)_T}\hat{\bar{T}}_F}{s + \frac{(hA)_T}{(Mc_p)_T}} - \hat{\bar{T}}_F\right) + \frac{(hA)_S}{(Mc_p)_F}\left(\frac{\frac{(hA)_S}{(Mc_p)_S}\hat{\bar{T}}_F + \frac{1}{(Mc_p)_S}\hat{P}}{s + \frac{(hA)_S}{(Mc_p)_S}} - \hat{\bar{T}}_F\right) \tag{11}$$

Solving for $\hat{\bar{T}}_F$:

$$\hat{\bar{T}}_F = \frac{\frac{1}{\tau_F}\hat{T}_{F,in} + \frac{(hA)_S}{(Mc_p)_F}\left(\frac{\frac{1}{(Mc_p)_S}}{s+\frac{(hA)_S}{(Mc_p)_S}}\right)\hat{P}}{s + \frac{1}{\tau_F} + \frac{(hA)_T}{(Mc_p)_F}\left(1 - \frac{\frac{(hA)_T}{(Mc_p)_T}}{s+\frac{(hA)_T}{(Mc_p)_T}}\right) + \frac{(hA)_S}{(Mc_p)_F}\left(1 - \frac{\frac{(hA)_S}{(Mc_p)_S}}{s+\frac{(hA)_S}{(Mc_p)_S}}\right)} \tag{12}$$

Using this result, we substitute (12) into (9) to get:

$$\hat{\bar{T}}_T = \frac{(hA)_T}{(Mc_p)_T}\frac{\frac{1}{\tau_F}\hat{T}_{F,in} + \frac{(hA)_S}{(Mc_p)_F}\left(\frac{\frac{1}{(Mc_p)_S}}{s+\frac{(hA)_S}{(Mc_p)_S}}\right)\hat{P}}{\left(s + \frac{(hA)_T}{(Mc_p)_T}\right)\left(s + \frac{1}{\tau_F} + \frac{(hA)_T}{(Mc_p)_F}\left(1 - \frac{\frac{(hA)_T}{(Mc_p)_T}}{s+\frac{(hA)_T}{(Mc_p)_T}}\right) + \frac{(hA)_S}{(Mc_p)_F}\left(1 - \frac{\frac{(hA)_S}{(Mc_p)_S}}{s+\frac{(hA)_S}{(Mc_p)_S}}\right)\right)} \tag{13}$$

And, finally, we substitute (12) into (10) to get:

$$\hat{\bar{T}}_S = \frac{(hA)_S}{(Mc_p)_S}\frac{\frac{1}{\tau_F}\hat{T}_{F,in} + \frac{(hA)_S}{(Mc_p)_F}\left(\frac{\frac{1}{(Mc_p)_S}}{s+\frac{(hA)_S}{(Mc_p)_S}}\right)\hat{P}}{\left(s + \frac{(hA)_S}{(Mc_p)_S}\right)\left(s + \frac{1}{\tau_F} + \frac{(hA)_T}{(Mc_p)_F}\left(1 - \frac{\frac{(hA)_T}{(Mc_p)_T}}{s+\frac{(hA)_T}{(Mc_p)_T}}\right) + \frac{(hA)_S}{(Mc_p)_F}\left(1 - \frac{\frac{(hA)_S}{(Mc_p)_S}}{s+\frac{(hA)_S}{(Mc_p)_S}}\right)\right)} + \frac{1}{(Mc_p)_S}\hat{P} \tag{14}$$

Now, to put each of these equations into a form so that they are linear combinations of $\hat{T}_{F,in}$ and $\hat{P}$,

$$\boxed{\begin{aligned}\hat{\hat{T}}_F(s) = {} & \frac{\frac{1}{\tau_F}}{s + \frac{1}{\tau_F} + \frac{(hA)_T}{(Mc_p)_F}\left(1 - \frac{\frac{(hA)_T}{(Mc_p)_T}}{s+\frac{(hA)_T}{(Mc_p)_T}}\right) + \frac{(hA)_S}{(Mc_p)_F}\left(1 - \frac{\frac{(hA)_S}{(Mc_p)_S}}{s+\frac{(hA)_S}{(Mc_p)_S}}\right)}\hat{T}_{F,in} + \\ & \frac{\frac{(hA)_S}{(Mc_p)_F}\left(\frac{\frac{1}{(Mc_p)_S}}{s+\frac{(hA)_S}{(Mc_p)_S}}\right)}{s + \frac{1}{\tau_F} + \frac{(hA)_T}{(Mc_p)_F}\left(1 - \frac{\frac{(hA)_T}{(Mc_p)_T}}{s+\frac{(hA)_T}{(Mc_p)_T}}\right) + \frac{(hA)_S}{(Mc_p)_F}\left(1 - \frac{\frac{(hA)_S}{(Mc_p)_S}}{s+\frac{(hA)_S}{(Mc_p)_S}}\right)}\hat{P}\end{aligned}} \tag{15}$$

$$\boxed{\begin{aligned}\hat{\hat{T}}_T(s) = {} & \frac{(hA)_T}{(Mc_p)_T}\frac{\frac{1}{\tau_F}}{\left(s + \frac{(hA)_T}{(Mc_p)_T}\right)\left(s + \frac{1}{\tau_F} + \frac{(hA)_T}{(Mc_p)_F}\left(1 - \frac{\frac{(hA)_T}{(Mc_p)_T}}{s+\frac{(hA)_T}{(Mc_p)_T}}\right) + \frac{(hA)_S}{(Mc_p)_F}\left(1 - \frac{\frac{(hA)_S}{(Mc_p)_S}}{s+\frac{(hA)_S}{(Mc_p)_S}}\right)\right)}\hat{T}_{F,in} + \\ & \frac{(hA)_T}{(Mc_p)_T}\frac{\frac{(hA)_S}{(Mc_p)_F}\left(\frac{\frac{1}{(Mc_p)_S}}{s+\frac{(hA)_S}{(Mc_p)_S}}\right)}{\left(s + \frac{(hA)_T}{(Mc_p)_T}\right)\left(s + \frac{1}{\tau_F} + \frac{(hA)_T}{(Mc_p)_F}\left(1 - \frac{\frac{(hA)_T}{(Mc_p)_T}}{s+\frac{(hA)_T}{(Mc_p)_T}}\right) + \frac{(hA)_S}{(Mc_p)_F}\left(1 - \frac{\frac{(hA)_S}{(Mc_p)_S}}{s+\frac{(hA)_S}{(Mc_p)_S}}\right)\right)}\hat{P}\end{aligned}} \tag{16}$$

$$\boxed{\begin{aligned}\hat{\hat{T}}_S(s) = {} & \frac{(hA)_S}{(Mc_p)_S}\frac{\frac{1}{\tau_F}}{\left(s + \frac{(hA)_S}{(Mc_p)_S}\right)\left(s + \frac{1}{\tau_F} + \frac{(hA)_T}{(Mc_p)_F}\left(1 - \frac{\frac{(hA)_T}{(Mc_p)_T}}{s+\frac{(hA)_T}{(Mc_p)_T}}\right) + \frac{(hA)_S}{(Mc_p)_F}\left(1 - \frac{\frac{(hA)_S}{(Mc_p)_S}}{s+\frac{(hA)_S}{(Mc_p)_S}}\right)\right)}\hat{T}_{F,in} + \\ & \left[\frac{(hA)_S}{(Mc_p)_S}\frac{\frac{(hA)_S}{(Mc_p)_F}\left(\frac{\frac{1}{(Mc_p)_S}}{s+\frac{(hA)_S}{(Mc_p)_S}}\right)}{\left(s + \frac{(hA)_S}{(Mc_p)_S}\right)\left(s + \frac{1}{\tau_F} + \frac{(hA)_T}{(Mc_p)_F}\left(1 - \frac{\frac{(hA)_T}{(Mc_p)_T}}{s+\frac{(hA)_T}{(Mc_p)_T}}\right) + \frac{(hA)_S}{(Mc_p)_F}\left(1 - \frac{\frac{(hA)_S}{(Mc_p)_S}}{s+\frac{(hA)_S}{(Mc_p)_S}}\right)\right)} + \frac{1}{(Mc_p)_S}\right]\hat{P}\end{aligned}} \tag{17}$$

Modeling the Heater More Simply

We begin by writing equations for the change in temperature for each section of the heater, divided into fluid and outer shell. (Here, to simplify, we assume that the inner tube will be the same temperature as the fluid, and we treat them collectively as one lumped thermal mass.)

$$\frac{d\bar{T}_F}{dt} = \frac{1}{\tau_F}(T_{F,in} - \bar{T}_F) + \frac{(hA)_S}{(Mc_p)_F}(\bar{T}_S - \bar{T}_F) \tag{24}$$

$$\frac{d\bar{T}_S}{dt} = \frac{(hA)_S}{(Mc_p)_S}(\bar{T}_F - \bar{T}_S) + \frac{P}{(Mc_p)_S} \tag{25}$$

where

- $\bar{T}_F$ = mean fluid temperature in "well-stirred tank" $[°C]$
- τ_F = transit time for fluid $[sec]$
- t = time $[sec]$
- $T_{F,in}$ = inlet fluid temperature $[°C]$
- $(Mc_p)_F$ = heat capacity of fluid $[kW \cdot sec/°C]$
- $(hA)_S$ = mean heat transfer times area for fluid-to-shell heat transfer $[kW/°C]$
- $\bar{T}_S$ = mean shell temperature $[°C]$
- P = power generation in heater outer shell $[kW]$
- $(Mc_p)_S$ = heat capacity of shell $[kW \cdot sec/°C]$

Now comes the fun part. In order to switch to the frequency domain, we use the relationship:

$$\frac{df}{dt} = sF(s) - f(0) \tag{26}$$

Assuming all of our variables are deviations from equilibrium values, we can then write:

$$s\hat{\bar{T}}_F = \frac{1}{\tau_F}(\hat{T}_{F,in} - \hat{\bar{T}}_F) + \frac{(hA)_S}{(Mc_p)_F}(\hat{\bar{T}}_S - \hat{\bar{T}}_F) \tag{27}$$

$$s\hat{\bar{T}}_S = \frac{(hA)_S}{(Mc_p)_S}(\hat{\bar{T}}_F - \hat{\bar{T}}_S) + \frac{\hat{P}}{(Mc_p)_S} \tag{28}$$

Solving the equations for their respective variables:

$$\hat{\bar{T}}_F = \frac{\frac{1}{\tau_F}\hat{T}_{F,in} + \frac{(hA)_S}{(Mc_p)_F}\hat{\bar{T}}_S}{s + \frac{1}{\tau_F} + \frac{(hA)_S}{(Mc_p)_F}} \tag{29}$$

$$\hat{\bar{T}}_S = \frac{\frac{(hA)_S}{(Mc_p)_S}\hat{\bar{T}}_F + \frac{1}{(Mc_p)_S}\hat{P}}{s + \frac{(hA)_S}{(Mc_p)_S}} \tag{30}$$

We can now substitute (30) into (29) to put $\hat{\bar{T}}_F$ into terms of the inputs $\hat{T}_{F,in}$ and $\hat{P}$ only:

$$\hat{\bar{T}}_F = \frac{\frac{1}{\tau_F}\hat{T}_{F,in} + \frac{(hA)_S}{(Mc_p)_F}\frac{\frac{(hA)_S}{(Mc_p)_S}\hat{\bar{T}}_F + \frac{1}{(Mc_p)_S}\hat{P}}{s+\frac{(hA)_S}{(Mc_p)_S}}}{s + \frac{1}{\tau_F} + \frac{(hA)_S}{(Mc_p)_F}} \tag{31}$$

$$\hat{\bar{T}}_F = \frac{\frac{1}{\tau_F}\hat{T}_{F,in} + \frac{(hA)_S}{(Mc_p)_F}\frac{\frac{1}{(Mc_p)_S}}{s+\frac{(hA)_S}{(Mc_p)_S}}\hat{P}}{\left(s + \frac{1}{\tau_F} + \frac{(hA)_S}{(Mc_p)_F}\right)\left(1 - \frac{(hA)_S}{(Mc_p)_F}\frac{\frac{(hA)_S}{(Mc_p)_S}}{s+\frac{(hA)_S}{(Mc_p)_S}}\right)} \tag{32}$$

Multiplying out and collecting like terms to get polynomials:

$$\hat{\bar{T}}_F = \frac{\frac{1}{\tau_F}\left[s + \frac{(hA)_S}{(Mc_p)_S}\right]\hat{T}_{F,in} + \frac{(hA)_S}{(Mc_p)_F(Mc_p)_S}\hat{P}}{s^2 + \left[\frac{1}{\tau_F} + \frac{(hA)_S}{(Mc_p)_F} + \frac{(hA)_S}{(Mc_p)_S}\right]s + \frac{(hA)_S}{(Mc_p)_S}\left(\frac{1}{\tau_F} - \frac{1}{\tau_F}\frac{(hA)_S}{(Mc_p)_F} + \frac{(hA)_S}{(Mc_p)_F} - \left[\frac{(hA)_S}{(Mc_p)_F}\right]^2\right)} \tag{33}$$

If we assume that the heater inlet temperature is at steady-state (because we control for CTAH outlet temperature), we can set the deviation from equilibrium to 0 and remove the $\hat{T}_{F,in}$ term and extract our transfer function for power to fluid temperature:

$$\boxed{\frac{\hat{\bar{T}}_F}{\hat{P}} = \frac{\frac{(hA)_S}{(Mc_p)_F(Mc_p)_S}}{s^2 + \left[\frac{1}{\tau_F} + \frac{(hA)_S}{(Mc_p)_F} + \frac{(hA)_S}{(Mc_p)_S}\right]s + \frac{(hA)_S}{(Mc_p)_S}\left(\frac{1}{\tau_F} - \frac{1}{\tau_F}\frac{(hA)_S}{(Mc_p)_F} + \frac{(hA)_S}{(Mc_p)_F} - \left[\frac{(hA)_S}{(Mc_p)_F}\right]^2\right)}} \tag{34}$$

We can follow a similar process for $\hat{T}_S$:

$$\hat{\bar{T}}_S = \frac{\frac{(hA)_S}{(Mc_p)_S}\frac{\frac{1}{\tau_F}\hat{T}_{F,in} + \frac{(hA)_S}{(Mc_p)_F}\hat{\bar{T}}_S}{s+\frac{1}{\tau_F}+\frac{(hA)_S}{(Mc_p)_F}} + \frac{1}{(Mc_p)_S}\hat{P}}{s + \frac{(hA)_S}{(Mc_p)_S}} \tag{35}$$

$$\hat{\bar{T}}_S = \frac{\frac{(hA)_S}{(Mc_p)_S}\frac{\frac{1}{\tau_F}\hat{T}_{F,in}}{s+\frac{1}{\tau_F}+\frac{(hA)_S}{(Mc_p)_F}} + \frac{1}{(Mc_p)_S}\hat{P}}{\left(s + \frac{(hA)_S}{(Mc_p)_S}\right)\left(1 - \frac{(hA)_S}{(Mc_p)_S}\frac{\frac{(hA)_S}{(Mc_p)_F}}{s+\frac{1}{\tau_F}+\frac{(hA)_S}{(Mc_p)_F}}\right)} \tag{36}$$

$$\hat{\bar{T}}_S = \frac{\frac{(hA)_S}{(Mc_p)_S}\frac{1}{\tau_F}\hat{T}_{F,in} + \frac{1}{(Mc_p)_S}\left(s + \frac{1}{\tau_F} + \frac{(hA)_S}{(Mc_p)_F}\right)\hat{P}}{s^2 + \left[\frac{(hA)_S}{(Mc_p)_S} + \frac{(hA)_S}{(Mc_p)_F} + \frac{1}{\tau_F} - \frac{(hA)_S}{(Mc_p)_S}\frac{(hA)_S}{(Mc_p)_F}\right]s + \frac{(hA)_S}{(Mc_p)_S}\left[\frac{(hA)_S}{(Mc_p)_F} + \frac{1}{\tau_F} - \frac{(hA)_S}{(Mc_p)_S}\frac{(hA)_S}{(Mc_p)_F}\right]} \tag{37}$$

Once again assuming that the heater inlet temperature is at steady-state:

$$\boxed{\frac{\hat{\bar{T}}_S}{\hat{P}} = \frac{\frac{1}{(Mc_p)_S}\left(s + \frac{1}{\tau_F} + \frac{(hA)_S}{(Mc_p)_F}\right)}{s^2 + \left[\frac{(hA)_S}{(Mc_p)_S} + \frac{(hA)_S}{(Mc_p)_F} + \frac{1}{\tau_F} - \frac{(hA)_S}{(Mc_p)_S}\frac{(hA)_S}{(Mc_p)_F}\right]s + \frac{(hA)_S}{(Mc_p)_S}\left[\frac{(hA)_S}{(Mc_p)_F} + \frac{1}{\tau_F} - \frac{(hA)_S}{(Mc_p)_S}\frac{(hA)_S}{(Mc_p)_F}\right]}} \tag{38}$$

Transfer Function Analysis

Fluid Now that we have these transfer functions, we can see what they tell us about our system. The zeros (roots of the numerator) and poles (roots of the denominator) give us important information at frequencies of interest.

Starting with equation (34), we see that we have no zeros but that we have poles. We factor the quadratic in the denominator to find our poles (I used WolframAlpha):

$$\frac{\hat{\bar{T}}_F}{\hat{P}} = \frac{(hA)_S}{(Mc_p)_F(Mc_p)_S} \frac{1}{\left(s + \frac{1}{\tau_F} + \frac{(hA)_S}{(Mc_p)_F}\right)\left(s + \left[\frac{(hA)_S}{(Mc_p)_F} - 1\right]\frac{(hA)_S}{(Mc_p)_S}\right)} \tag{39}$$

which means that we have poles at:

$$\boxed{p_1 = -\frac{1}{\tau_F} - \frac{(hA)_S}{(Mc_p)_F} \quad , \quad p_2 = -\left[\frac{(hA)_S}{(Mc_p)_F} - 1\right]\frac{(hA)_S}{(Mc_p)_S}}$$

and we can calculate our static gain by setting $s = 0$:

$$\boxed{K = \frac{1}{(Mc_p)_F\left(\frac{1}{\tau_F} + \frac{(hA)_S}{(Mc_p)_F}\right)\left(\frac{(hA)_S}{(Mc_p)_F} - 1\right)}}$$

giving us the standard Bode form (to facilitate plotting):

$$\boxed{\frac{\hat{\bar{T}}_F}{\hat{P}} = \frac{1}{(Mc_p)_F\left(\frac{1}{\tau_F} + \frac{(hA)_S}{(Mc_p)_F}\right)\left(\frac{(hA)_S}{(Mc_p)_F} - 1\right)} \frac{1}{\left(\frac{s}{\frac{1}{\tau_F} + \frac{(hA)_S}{(Mc_p)_F}} + 1\right)\left(\frac{s}{\left[\frac{(hA)_S}{(Mc_p)_F} - 1\right]\frac{(hA)_S}{(Mc_p)_S}} + 1\right)}} \tag{40}$$

Because we know that all of our parameters are real, nonzero, positive values, we know that we have a real pole at p_1 and a real pole at p_2 as long as convective heat transfer to the heater outer shell is of greater magnitude than the thermal mass of the fluid. On a Bode magnitude plot of this frequency response, each real pole decreases the slope of the magnitude by 20 dB. We will also see static gain K on the Bode magnitude plot of the frequency response at frequencies below p_1 and p_2.

Shell Similarly, for the shell:

$$\frac{\hat{\bar{T}}_S}{\hat{P}} = \frac{1}{(Mc_p)_S} \frac{s + \frac{1}{\tau_F} + \frac{(hA)_S}{(Mc_p)_F}}{\left(s + \frac{(hA)_S}{(Mc_p)_S}\right)\left(s - \left[\frac{(hA)_S}{(Mc_p)_S} - 1\right]\frac{(hA)_S}{(Mc_p)_F} + \frac{1}{\tau_F}\right)} \tag{41}$$

which means we have a zero at:

$$\boxed{z_1 = -\frac{1}{\tau_F} - \frac{(hA)_S}{(Mc_p)_F}}$$

poles at:

$$\boxed{p_1 = -\frac{(hA)_S}{(Mc_p)_S} \quad , \quad p_2 = \left[\frac{(hA)_S}{(Mc_p)_S} - 1\right]\frac{(hA)_S}{(Mc_p)_F} - \frac{1}{\tau_F}}$$

and a static gain of:

$$\boxed{K = \frac{\frac{1}{\tau_F} + \frac{(hA)_S}{(Mc_p)_F}}{(hA)_S\left(\frac{1}{\tau_F} - \left[\frac{(hA)_S}{(Mc_p)_S} - 1\right]\frac{(hA)_S}{(Mc_p)_F}\right)}}$$

yielding a Bode form of:

$$\boxed{\frac{\hat{\bar{T}}_S}{\hat{P}} = \frac{\frac{1}{\tau_F} + \frac{(hA)_S}{(Mc_p)_F}}{(hA)_S\left(\frac{1}{\tau_F} - \left[\frac{(hA)_S}{(Mc_p)_S} - 1\right]\frac{(hA)_S}{(Mc_p)_F}\right)} \frac{\frac{s}{\frac{1}{\tau_F} + \frac{(hA)_S}{(Mc_p)_F}} + 1}{\left(\frac{s}{\left[\frac{(hA)_S}{(Mc_p)_S}\right]} + 1\right)\left(\frac{s}{\frac{1}{\tau_F} - \left[\frac{(hA)_S}{(Mc_p)_S} - 1\right]\frac{(hA)_S}{(Mc_p)_F}} + 1\right)}} \tag{42}$$

Because we don't know these values, this doesn't allow us to numerically create Bode magnitude plots for these transfer functions. However, we can make theoretical Bode magnitude plots that we can compare with experimentally-derived plots in order to identify our K, z, and p values with numerical values.